

Progress and Challenges in Targeting the SARS-CoV-2 Papain-like Protease

Haozhou Tan, Yanmei Hu, Prakash Jadhav, Bin Tan, and Jun Wang*

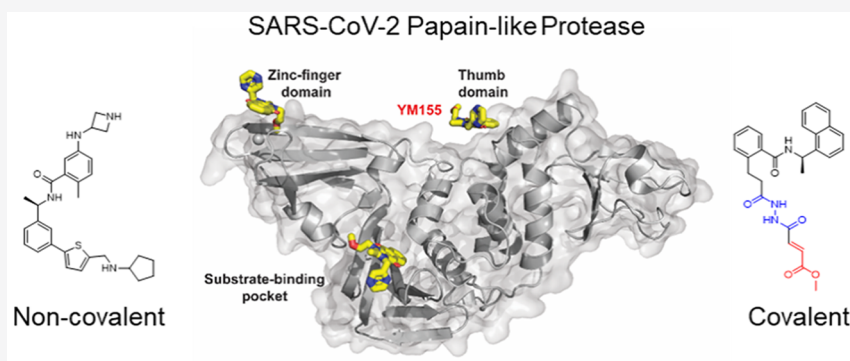
Cite This: *J. Med. Chem.* 2022, 65, 7561–7580

Read Online

ACCESS |

Metrics & More

Article Recommendations



ABSTRACT: SARS-CoV-2 is the causative agent of the COVID-19 pandemic. The approval of vaccines and small-molecule antivirals is vital in combating the pandemic. The viral polymerase inhibitors remdesivir and molnupiravir and the viral main protease inhibitor nirmatrelvir/ritonavir have been approved by the U.S. FDA. However, the emergence of variants of concern/interest calls for additional antivirals with novel mechanisms of action. The SARS-CoV-2 papain-like protease (PL^{Pro}) mediates the cleavage of viral polyprotein and modulates the host's innate immune response upon viral infection, rendering it a promising antiviral drug target. This Perspective highlights major achievements in structure-based design and high-throughput screening of SARS-CoV-2 PL^{Pro} inhibitors since the beginning of the pandemic. Encouraging progress includes the design of non-covalent PL^{Pro} inhibitors with favorable pharmacokinetic properties and the first-in-class covalent PL^{Pro} inhibitors. In addition, we offer our opinion on the knowledge gaps that need to be filled to advance PL^{Pro} inhibitors to the clinic.

1. INTRODUCTION

Coronaviruses (CoVs) are enveloped, positive-sense, and single-stranded RNA (+ssRNA) viruses. CoVs belong to the subfamily Orthocoronavirinae, family Coronaviridae, and order Nidovirales. Seven coronaviruses are known to infect humans: four common human coronaviruses—HCoV-229E, HCoV-NL63, HCoV-OC43, and HCoV-HKU1—that cause mild symptoms¹ and three coronaviruses—SARS-CoV, MERS-CoV, and SARS-CoV-2—that cause severe acute respiratory tract infections.^{2,3} Although humans around the world are commonly infected with HCoV-229E, HCoV-NL63, HCoV-OC43, or HCoV-HKU1, the infection generally only causes mild symptoms that do not require medical treatments.^{4,5} Accordingly, no major efforts have been devoted to developing vaccines and antiviral drugs against these viruses. Nonetheless, the 21st century witnessed several coronavirus outbreaks that raised the alarm regarding this virus family. In late 2002, SARS-CoV emerged in Guangdong, China, and caused approximately 8000 cases, with a fatality rate of 9.6%.⁶ In 2012, MERS-CoV emerged in Saudi Arabia and South Korea, causing approximately 2400 cases in the following 8 years, with a fatality rate of 34%.⁷

Notably, in 2019, SARS-CoV-2 emerged in Hubei, China, and quickly ramped up to the coronavirus disease 2019 (COVID-19) pandemic.^{8,9} The clinical outcomes of COVID-19 range from non-symptomatic, mild to severe respiratory tract infections, and influenza-like illness, to lung injuries, organ failure, and death.¹⁰ To date, SARS-CoV-2 has spread all over the world and is the most severe pandemic in recent history. As of May 3, 2022, 511 million cases and 6.23 million deaths had been reported worldwide, among which the United States has had 80.5 million cases and 986,298 deaths.¹¹

Given the devastating impact of COVID-19 on social life, public health, and the global economy, researchers around the world are working relentlessly to develop countermeasures. This

Received: February 24, 2022

Published: May 27, 2022



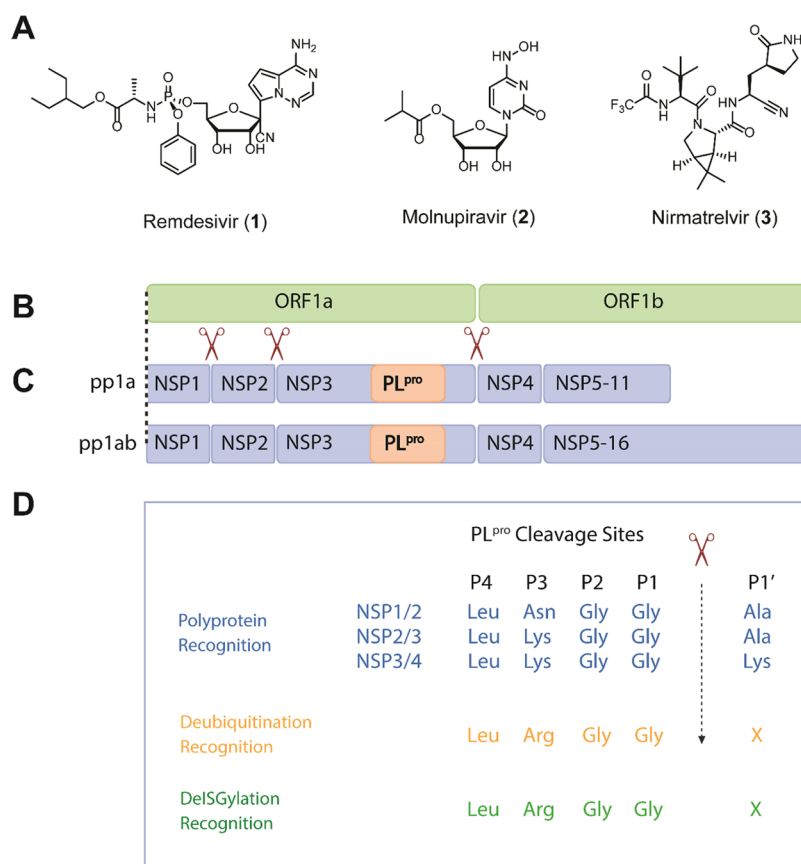


Figure 1. Chemical structures of FDA-approved COVID-19 antiviral drugs (A) and the schematic representation of the SARS-CoV and SARS-CoV-2 Open Reading Frame (B), the polyprotein replicase (C), and the recognition motifs of PL^{pro} (D). The genome contains two open reading frames, ORF1a and ORF1b, which are directly translated into polyproteins pp1a and pp1ab due to the ribosomal frameshift between the two ORFs. pp1a contains 11 NSPs, and pp1ab contains 16 NSPs. The PL^{pro} is located within the NSP3. The polyproteins are processed into functional NSP units through cleavage by PL^{pro} and M^{pro}, and the cleavage sites of PL^{pro} are shown in (C). The substrate amino acid sequence alignment of P4–P1' recognized by PL^{pro} is shown in (D).

effort has led to the development of vaccines and antiviral drugs in record-breaking times.^{12,13} Vaccines mainly target the viral surface spike protein and rely on the production of antibodies to block the viral entry through inhibiting the interaction between the viral spike protein and the host cell angiotensin converting enzyme 2 (ACE2) receptor.¹⁴ Three vaccines received approval from the U.S. Food and Drug Administration (FDA), including two mRNA vaccines, from Pfizer/BioNTech (Comirnaty) and Moderna (Spikevax), and one adenovirus-based vaccine, from Johnson & Johnson/Janssen. In addition, several vaccines from China and Russia have been approved by the World Health Organization (WHO).¹⁵

For small-molecule antivirals, major progress has been made in targeting the SARS-CoV-2 RNA-dependent RNA polymerase (RdRp), the main protease (M^{pro} or 3CL^{pro}), and the papain-like protease (PL^{pro}).^{16,17} The first RdRp inhibitor, remdesivir (1, Figure 1A), was identified from a drug repurposing approach and approved for the treatment of severe SARS-CoV-2 infection by intravenous (i.v.) administration.¹⁸ Remdesivir acts as a chain terminator during viral RNA synthesis.¹⁹ Similarly, the second RdRp inhibitor, molnupiravir (2, Figure 1A) was originally developed as an influenza antiviral and was later shown to have broad-spectrum antiviral activity against several viruses, including SARS-CoV-2.^{20,21} Molnupiravir (2) is a mutagen, and when incorporated into the RNA chain, it increases the mutation rate of the virus.²² Molnupiravir (2) is a prodrug and

has the advantage of oral administration.²³ The main protease inhibitor, Paxlovid, developed by Pfizer, is a combination of nirmatrelvir (3, Figure 1A) and ritonavir.¹³ Nirmatrelvir (3) is an M^{pro} inhibitor, and ritonavir is included as a boosting agent to increase the half-life of nirmatrelvir. A similar approach was explored in the HIV drug combination Kaletra (lopinavir + ritonavir). Ritonavir is an inhibitor of cytochrome P450 3A4 (CYP3A4), and co-administration of ritonavir is required to increase the *in vivo* concentration of nirmatrelvir (3) to the target therapeutic range.

The approvals of vaccines and RdRp and M^{pro} inhibitors are encouraging signs to combat the COVID-19 pandemic and possibly return to the pre-pandemic normalcy.²⁴ However, the emergence of SARS-CoV-2 variants of concern (VOC) and variants of interests (VOI) poses a pressing need for additional vaccines and antiviral drugs.²⁵ Multiple studies have shown the reduced efficacy of vaccines against Omicron VOC.^{26,27} Drug-resistant mutations have been evolved against remdesivir (1) in cell culture through serial passage experiments^{28,29} as well as in an immunocompromised patient.³⁰ In addition, the therapeutic benefits of remdesivir (1) are still under debate from several clinical trials.^{31,32} Molnupiravir (2) has the potential risk of inducing mutations in the host, which is pending validation.^{33,34} Molnupiravir (2) was shown to be positive in the Ames test,³⁵ which is a standard assay to measure mutagenic potential of drug candidates in bacteria. β -D-N⁴-Hydroxycytidine (NHC), the

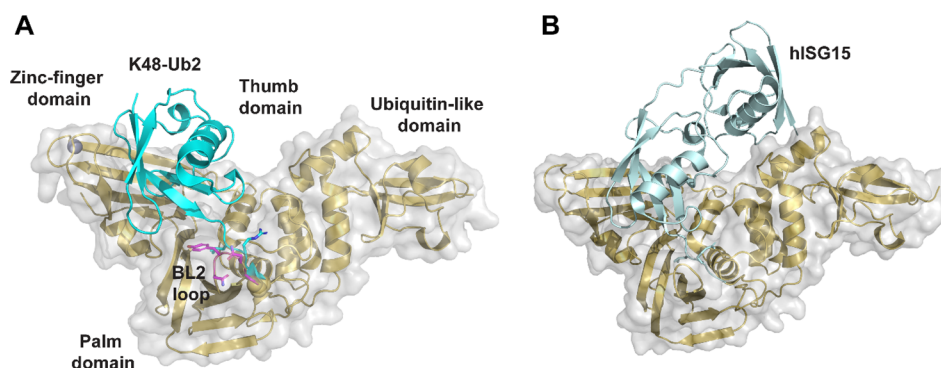


Figure 2. X-ray crystal structures of SARS-CoV-2 PL^{pro}. (A) X-ray crystal structure of SARS-CoV-2 PL^{pro} C111S mutant with K48-linked Ub2 (PDB: 7RBR). The BL2 loop is colored in magenta. (B) X-ray crystal structure of SARS-CoV-2 PL^{pro} C111S mutant with human ISG15 (PDB: 7RBS).⁵⁶

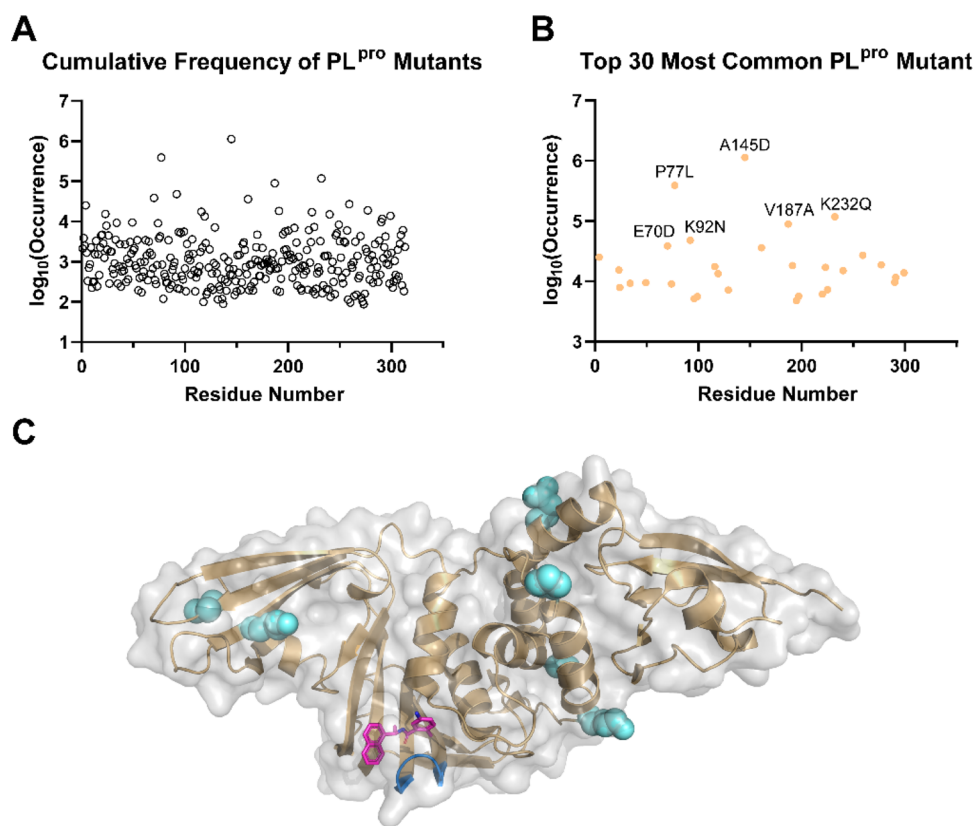


Figure 3. Analysis of SARS-CoV-2 PL^{pro} mutations. Based on the data retrieved from GISAID (www.gisaid.org/epiflu-applications/covsurver-mutations-app), 2,487,047 sequences that contains mutations on PL^{pro} have been identified, which fall into 5754 different types of mutations on various positions of PL^{pro}. All numbers shown are accurate as of Jan 25, 2022. (A) Cumulative frequency of SARS-CoV-2 PL^{pro} mutants. (B) The top 30 most common SARS-CoV-2 PL^{pro} mutants. Among these mutants, A145 has the most frequent mutation to D with 1,131,252 occurrences (99.8% on 145); P77L with 372,993 occurrences (95.7% on 77); K232Q with 117,247 occurrences (99.1% on 232); V187A with 87,861 occurrences (97.9% on 187); and K92N with 47,110 occurrences (98.2%). (C) Mapping of the top six SARS-CoV-2 PL^{pro} mutants to the X-ray crystal structure of PL^{pro} in complex with GRL0617 (4) (PDB: 7JRN). The residues are shown as spheres. The BL2 loop in the drug-binding site is colored in marine, and the drug GRL0617 (4) is colored in magenta.

active metabolite of molnupiravir (2), displayed host mutational activity in mammalian cell culture.³⁴ Multiple mutations have been identified in M^{pro} among the SARS-CoV-2 VOC and VOI, including the Omicron M^{pro} P132H mutant.³⁶ Although the currently identified M^{pro} mutants remain sensitive to nirmatrelvir (3),^{36–38} the scientific community is on high alert for future mutations, such as H172Y and S144A, that might lead to drug resistance.³⁹ The genetic barrier to resistance for protease inhibitors is generally moderate to low, as shown by HIV and HCV protease inhibitors.⁴⁰ Resistance to Paxlovid is expected to

rise with the increasing prescription. In addition, nirmatrelvir (3) is used in combination with ritonavir in clinics to prolong its half-life. Ritonavir is a potent inhibitor of the CYP3A4 isoenzyme and thus poses the risk of drug–drug interactions.⁴¹ As such, additional antivirals with a novel mechanism of action are clearly needed to combat emerging variants and drug-resistant viruses. In this regard, the SARS-CoV-2 PL^{pro} stands out as one of the next-in-line high-profile drug targets.

PL^{pro} and the M^{pro} are the two essential proteases encoded by the SARS-CoV-2 genome. Both PL^{pro} and M^{pro} cleave the

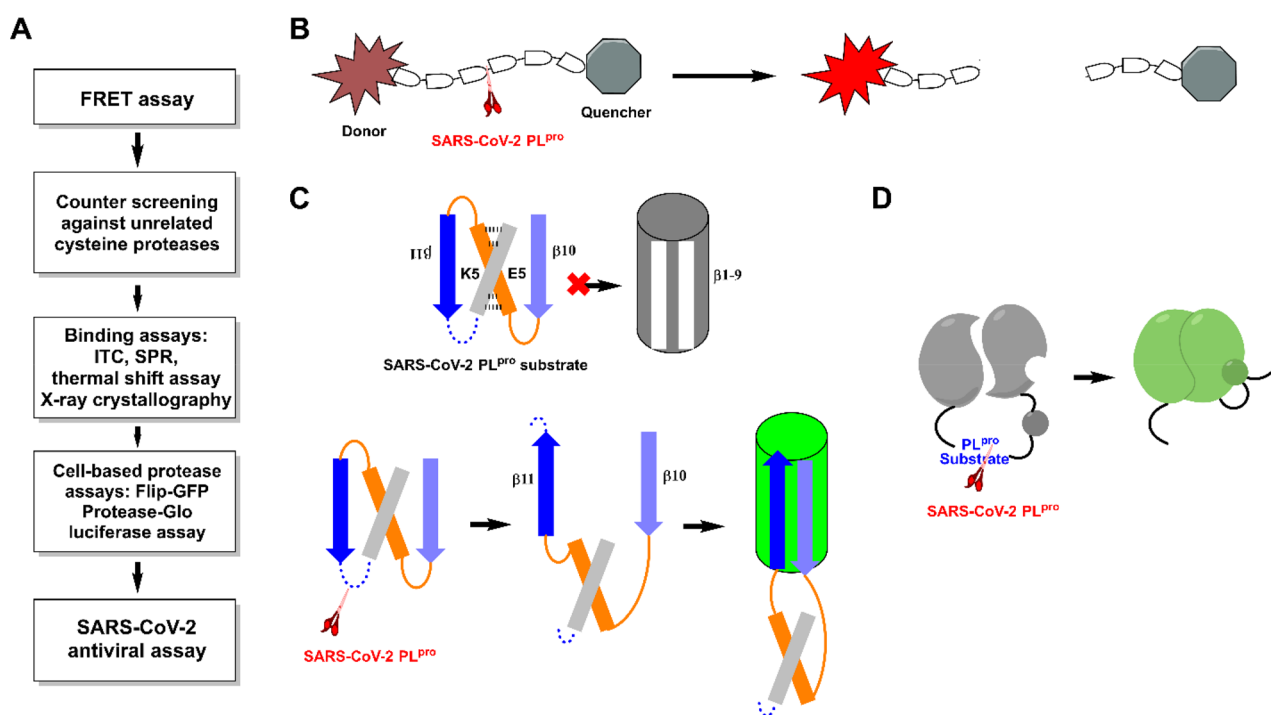


Figure 4. SARS-CoV-2 PL^{pro} assays. (A) General flowchart for the pharmacological characterization of PL^{pro} inhibitors. (B) Assay principle for the FRET-based enzymatic assay. (C) Assay principle for the cell-based FlipGFP PL^{pro} assay. (D) Assay principle for the Protease-Glo luciferase PL^{pro} assay.

peptide bonds in the viral polyprotein to release functional non-structural proteins (NSPs) for viral transcription and replication. In addition, PL^{pro} is involved in antagonizing the host's immune response upon viral infection. PL^{pro} has deubiquitinating and deISGylating activities and removes ubiquitin and ISG15 modifications from host proteins, leading to suppression of the innate immune response and promotion of viral replication.^{42–44} The deubiquitinating and deISGylating activities of PL^{pro} are indispensable in antagonizing the host's immune response.^{45,46} Recent studies showed that SARS-CoV-2 infection of human macrophages triggers the release of extracellular free ISG15 through the viral PL^{pro}, leading to the subsequent secretion of proinflammatory cytokines and chemokines, which recapitulates the cytokine storm of COVID-19.^{47,48} This finding suggests that inhibiting the PL^{pro} activity might alleviate the hyper-inflammation in COVID patients. Thus, targeting PL^{pro} is expected to not only suppress viral replication but also restore antiviral immunity in the host.⁴⁵

There are two types of PL^{pro}s: PL1^{pro} and PL2^{pro}.^{49,50} The viruses HCoV-229E, HCoV-NL63, HCoV-HKU1, and HCoV-OC43 encode both PL1^{pro} and PL2^{pro}. PL1^{pro} and PL2^{pro} have distinct substrate specificities in different coronaviruses.⁵¹ In contrast, SARS-CoV, MERS-CoV, and SARS-CoV-2 comprise only one functional PL2^{pro}.

PL^{pro} is part of the nsp3, a 215-kDa multidomain viral protein. SARS-CoV-2 PL^{pro} specifically recognizes a consensus cleavage motif, LXGG↓(N/K/X), which is present in between nsp1/2, nsp2/3, and nsp3/4 at the viral polyprotein as well as the C-terminal sequences of ubiquitin and ISG15 with an isopeptide bond (Figure 1B–D).

The SARS-CoV-2 PL^{pro} contains four domains: the thumb, palm, zinc-finger domain, and an N-terminal ubiquitin-like domain (Figure 2). The catalytic triad consists of Cys111, His272, and Asp286, which are located at the interface of the

palm and thumb domains. The zinc-finger motif comprises four cysteines coordinating with a zinc ion and is vital for the structural integrity and the protease activity of PL^{pro}. The flexible BL2 loop undergoes conformational changes from open to closed upon substrate binding (Figure 2A).⁵² This site is also the drug-binding site for GRL0617 (4) and its analogues.¹⁶ The X-ray crystal structures for the apo SARS-CoV-2 PL^{pro}, drug-bound form,^{52–55} and complex forms with ubiquitin (Figure 2A) and ISG15 (Figure 2B) have been solved,⁵⁶ paving the way for structure-based drug design and understanding the virology of PL^{pro}.

SARS-CoV-2 PL^{pro} shares a sequence identity of 82.9% with SARS-CoV PL^{pro} and, to a lesser extent, 32.9% identity with MERS-CoV PL^{pro}. Despite the high sequence similarity, SARS-CoV-2 PL^{pro} has enhanced deISGylating activity and reduced deubiquitinating activity compared to SARS-CoV PL^{pro}.^{45,46,57} PL^{pro} is a conserved drug target among SARS-CoV-2 variants (Figure 3). Although mutations have been identified, top high-frequency mutations are all located distal from the drug-binding site (Figure 3C). Nonetheless, it remains to be experimentally validated whether these mutations will alter drug sensitivity. In addition, resistance might emerge under drug selection pressure.

The knowledge accumulated through studying SARS-CoV PL^{pro} provides a foundation for understanding the virology of SARS-CoV-2 PL^{pro} and developing SARS-CoV-2 PL^{pro} inhibitors. For excellent reviews and research articles of the structure, function, and inhibition of SARS-CoV PL^{pro}, please refer to previous publications.^{16,58–62} This Perspective covers recent advances in the development of SARS-CoV-2 PL^{pro} inhibitors and their mechanism of action. We also discuss the knowledge gaps that need to be filled to advance PL^{pro} inhibitors to clinic.

It is not the objective of this Perspective to enumerate all SARS-CoV-2 PL^{pro} inhibitors reported in the literature; instead, the focus is on highlighting several well-characterized examples.

Table 1. SARS-CoV-2 PL^{pro} Inhibitors⁴⁷

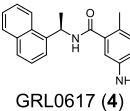
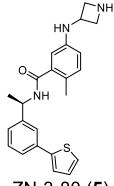
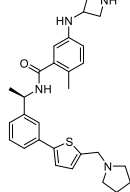
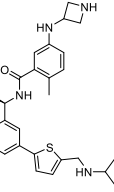
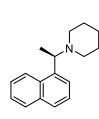
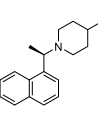
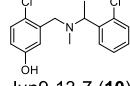
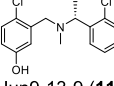
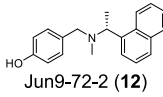
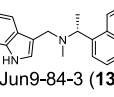
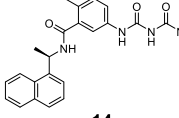
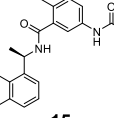
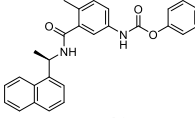
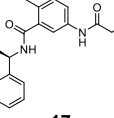
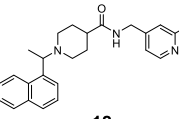
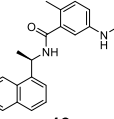
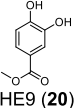
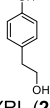
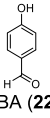
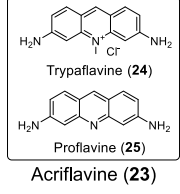
Structure	Enzymatic inhibition IC ₅₀ (μM)	Antiviral EC ₅₀ /CC ₅₀ (μM)	Structure	Enzymatic inhibition IC ₅₀ (μM)	Antiviral EC ₅₀ /CC ₅₀ (μM)
Non-covalent SARS-CoV-2 PL^{pro} inhibitors – GRL0617 analogues					
 GRL0617 (4)	1.39 ± 0.26 ⁸⁰ 1.789 ⁸¹	3.18 ± 0.71~500 ⁸⁰ 32.64 ⁸¹ > 20 ⁸⁷	 ZN-3-80 (5)	0.59 ± 0.04 ⁶⁷ K _D = 0.963 μM (SPR)	N.T.
 XR8-24 (6)	0.56 ± 0.03 ⁶⁷ K _D = 0.372 μM (SPR) PDB: 7LBS	1.2 ± 0.2	 XR8-23 (7)	0.39 ± 0.05 ⁶⁷ K _D = 0.235 μM (SPR)	1.4 ± 0.1
 8	0.44 ± 0.05 ⁷⁹ K _D = 2.60 ± 0.39 μM (SPR)	0.18 ± 0.10 CC ₅₀ > 10	 9	2.69 ± 0.34 ⁷⁹ PDB: 7E35	N.T.
 Jun9-13-7 (10)	7.29 ± 1.03 ⁵⁴	N.T.	 Jun9-13-9 (11)	6.67 ± 0.55 ⁵⁴	N.T.
 Jun9-72-2 (12)	0.67 ± 0.08 ⁵⁴ PDB: 7SDR	6.62 ± 1.31 (Vero) 7.90 ± 2.40 (Caco-2 hACE2)	 Jun9-84-3 (13)	0.67 ± 0.14 ⁵⁴ PDB: 7SQE	8.31 ± 2.68 (Vero) 11.99 ± 4.52 (Caco-2 hACE2)
 14	5.1 ± 0.7 ⁵² GRL0617 (4) (2.3 ± 0.2) PDB: 7JIT	Not active	 15	6.4 ± 0.6 ⁵² PDB: 7JIV, 7JIW	Not active
 16	7.0 ± 0.6 ⁵²	Not active	 17	12.7 ± 1.3 ⁵²	5.2 ± 4.2 (Vero E6)
 18	0.81 ⁵³	< 11 μM	 19	11 ± 3 ⁶⁸ GRL0617 (4) (2.1 ± 0.2)	N.T.
Non-covalent SARS-CoV-2 PL^{pro} inhibitors – Non-GRL0617 analogues					
 HE9 (20)	3.76 ± 1.13 ⁵⁵ (ISG15-Rh substrate) PDB: 7OFU	0.13 (qRT-PCR) 10 (CPE)	 YRL (21)	6.68 ± 1.20 ⁵⁵ (ISG15-Rh substrate) PDB: 7OFS	1 (qRT-PCR) Not active (CPE)
 HBA (22)	3.99 ± 1.33 ⁵⁵ (ISG15-Rh substrate) PDB: 7OFT	Not active (CPE)	 Trypaflavine (24) Proflavine (25) Acriflavine (23)	1.66 (RLRGG-AMC) ⁸² 1.46 (ISG15-AMC) PDB: 7NT4	A549/ACE2 EC ₅₀ = 86 nM, CC ₅₀ = 3.1 μM SI = 36 Vero EC ₅₀ = 64 nM, CC ₅₀ = 3.4 μM SI = 53

Table 1. continued

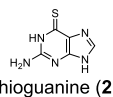
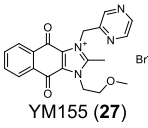
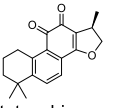
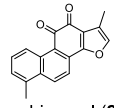
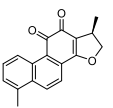
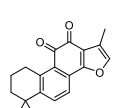
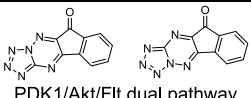
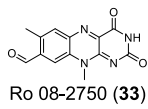
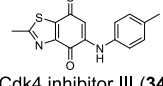
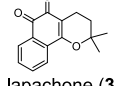
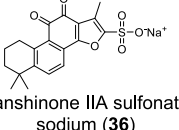

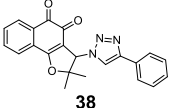
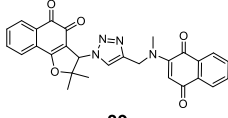
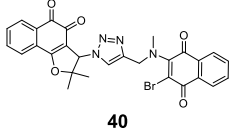
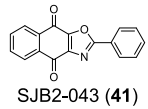
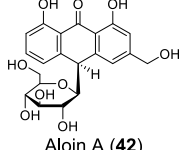
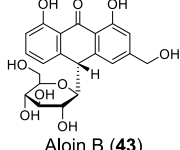
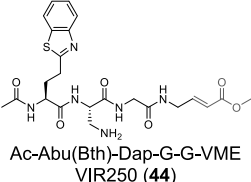
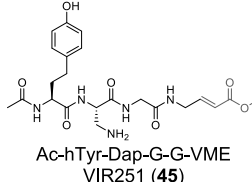
Structure	Enzymatic inhibition IC ₅₀ (μM)	Antiviral EC ₅₀ /CC ₅₀ (μM)	Structure	Enzymatic inhibition IC ₅₀ (μM)	Antiviral EC ₅₀ /CC ₅₀ (μM)
 6-thioguanine (26)	0.5 (TAP-nsp123) 1.0 (TAP-nap23) 0.1 (de-ISGylation) 72 ± 12 ⁹⁴	2.13 ± 1.16/35.5 ± 9.45 (Vero E6)	 YM155 (27)	2.47 ± 0.46 ⁹⁰ Assay condition: 50 mM HEPES, pH 7.5, 2 mM DTT PDB: 7D7L	0.17 ± 0.02/~400 ⁹⁰
 Cryptotanshinone (28)	5.63 ± 1.45 ⁹⁰ 1.336 ⁸¹	0.70 ± 0.09/>300 ⁹⁰ >200 ⁸¹	 Tanshinone I (29)	2.21 ± 0.10 ⁹⁰	2.26 ± 0.11/>200 ⁹⁰
 Dihydrotanshinone I (30)	0.59 ⁸¹	8.15 ⁸¹	 Tanshinone IIA (31)	1.571 ⁸¹	>200 ⁸¹
 PDK1/Akt/Fit dual pathway inhibitor (32)	0.26 ⁸¹	N.T.	 Ro 08-2750 (33)	0.53 ⁸¹	20
 Cdk4 inhibitor III (34)	0.39 ⁸¹	cytotoxic	 β-lapachone (35)	0.61 ⁸¹	cytotoxic
 Tanshinone IIA sulfonate sodium (36)	1.65 ± 0.13 ⁸³ K _D = 61.0 ± 12.1 μM (BLI assay)	N.T.	 Chloroxine (37)	7.24 ± 0.68 ⁸³ (FP assay) K _D = 4.6 ± 0.29 μM (BLI assay)	N.T.
 38	1.7 ⁸⁴	Not active	 39	2.2 ⁸⁴	Not active
 40	3.1 ⁸⁴ M ^{pro} (IC ₅₀ = 66 μM)	Not active	 SJB2-043 (41)	0.56 ± 0.16 ⁸⁵	N.T.
 Aloin A (42)	13.16 ⁸⁶ 15.68 (DUB)	N.T. CC ₅₀ > 100 μM (Vero E6)	 Aloin B (43)	16.08 ⁸⁶ 17.51 (DUB)	N.T. CC ₅₀ > 100 μM (Vero E6)
Covalent SARS-CoV-2 PL^{pro} inhibitors					
 Ac-Abu(Bth)-Dap-G-G-VME VIR250 (44)	Near complete inhibition at 100 μM ⁵⁷ PDB: 6WUU	N.T.	 Ac-hTyr-Dap-G-G-VME VIR251 (45)	Near complete inhibition at 100 μM ⁵⁷ PDB: 6WX4	N.T.

Table 1. continued

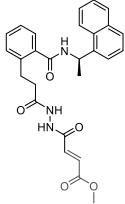
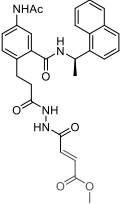
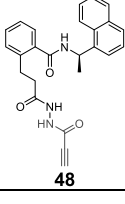
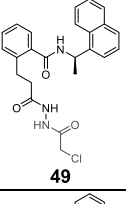
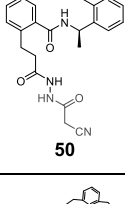
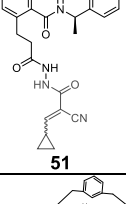
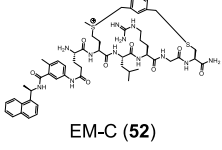
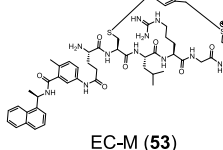
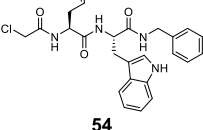
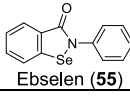
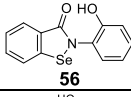
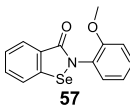
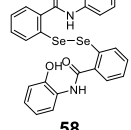
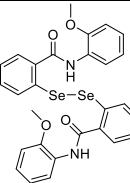
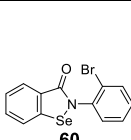
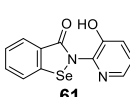
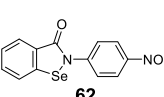
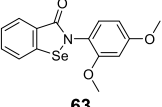
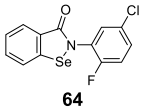
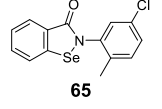
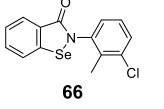
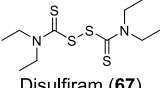
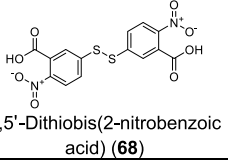
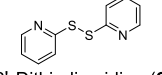
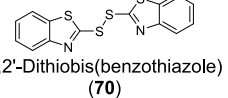
Structure	Enzymatic inhibition IC ₅₀ (μM)	Antiviral EC ₅₀ /CC ₅₀ (μM)	Structure	Enzymatic inhibition IC ₅₀ (μM)	Antiviral EC ₅₀ /CC ₅₀ (μM)
 46	0.094 ⁸⁷ K _{inact} /K _i =10,000 M ⁻¹ S ⁻¹	1.1	 47	0.230 ⁸⁷ K _{inact} /K _i =14,000 M ⁻¹ S ⁻¹	Not active
 48	0.098 ⁸⁷ K _{inact} /K _i =4,800 M ⁻¹ S ⁻¹	Cytotoxic	 49	5.4 ⁸⁷ K _{inact} /K _i =103 M ⁻¹ S ⁻¹	34
 50	8.0 ⁸⁷	Not active	 51	> 200 ⁸⁷	Cytotoxic
 EM-C (52)	7.40 ± 0.37 ⁸⁸	N.T.	 EC-M (53)	8.63 ± 0.55 ⁸⁸	N.T.
 54	0.67 ⁸⁹ M ^{pro} (IC ₅₀ = 1.72 μM)	0.32 (UC-1074) 1.37 (UC-1075)			
Ebselen analogues					
 Ebselen (55)	2.02 ± 1.02 ⁹⁰	N.T.	 56	0.236 ± 0.107 ⁹⁰	N.T.
 57	0.256 ± 0.035 ⁹⁰	N.T.	 58	0.339 ± 0.109 ⁹⁰	N.T.
 59	0.263 ± 0.121 ⁹⁰	N.T.	 60	PL ^{pro} IC ₅₀ = 1.255 ± 0.095 μM ⁹¹ M ^{pro} IC ₅₀ = 25.69 ± 2.64 nM	N.T.
 61	PL ^{pro} IC ₅₀ = 0.578 ± 0.040 μM M ^{pro} 91 IC ₅₀ = 49.55 ± 2.95 nM	N.T.	 62	PL ^{pro} IC ₅₀ = 1.885 ± 0.098 μM M ^{pro} 91 IC ₅₀ = 27.95 ± 5.10 nM	N.T.

Table 1. continued

Structure	Enzymatic inhibition IC ₅₀ (μM)	Antiviral EC ₅₀ /CC ₅₀ (μM)	Structure	Enzymatic inhibition IC ₅₀ (μM)	Antiviral EC ₅₀ /CC ₅₀ (μM)
 63	PL ^{pro} IC ₅₀ = 0.990 ± 0.058 μM M ^{pro} 91 IC ₅₀ = 52.50 ± 4.51 nM	N.T.	 64	PL ^{pro} IC ₅₀ = 2.067 ± 0.078 μM M ^{pro} 91 IC ₅₀ = 15.24 ± 4.58 nM	N.T.
 65	PL ^{pro} IC ₅₀ = 1.038 ± 0.083 μM M ^{pro} 91 IC ₅₀ = 37.81 ± 3.28 nM	N.T.	 66	PL ^{pro} IC ₅₀ = 1.288 ± 0.052 μM M ^{pro} 91 IC ₅₀ = 27.37 ± 2.35 nM	N.T.
Zinc ejectors					
 Disulfiram (67)	7.52 ± 2.13 ¹⁰⁰	N.T.	 5,5'-Dithiobis(2-nitrobenzoic acid) (68)	N.T.	N.T.
 2,2'-Dithiodipyridine (69)	N.T.	N.T.	 2,2'-Dithiobis(benzothiazole) (70)	N.T.	N.T.

^aN.T. = not tested.

Non-specific PL^{pro} inhibitors will also be discussed with the intention to alert the scientific community.

2. SARS-CoV-2 PL^{pro} ASSAYS

Vigorous pharmacological characterization is vital in triaging non-specific inhibitors at the early stage and prioritizing hits with translational potential for further development. For this, we provide a brief introduction of the commonly used assays for the pharmacological characterization of PL^{pro} inhibitors (Figure 4A).

The gold standard assay for protease is the fluorescence resonance energy transfer (FRET)-based enzymatic assay, which is typically used as a primary assay for compound testing. In the FRET assay, a peptide corresponding to the protease substrate is designed with a fluorophore donor and a quencher at the two ends (Figure 4B). Upon cleavage by the protease, an increase in fluorescence signal is observed. However, the enzymatic assay condition varies among different laboratories in terms of enzyme concentration, FRET substrate sequence, pH, the addition of detergent (to rule out aggregates), bovine serum albumin (to rule out non-specific hydrophobic interactions), and reducing reagent (to prevent non-specific modification of catalytic Cys111). For this reason, the IC₅₀ values from different studies should be interpreted with caution and should not be used for direct comparison. Instead, positive controls such as GRL0617 (**4**) need to be included as a reference to normalize the results. The assay guidance manual compiled by Eli Lilly & Company and the National Center for Advancing Translational Sciences offers detailed guidance for assay optimization, which might help limit the variations between individual laboratories.⁶⁵ In addition, counter screening against unrelated cysteine proteases should be conducted to rule out non-specific inhibitors. Furthermore, compounds that either quench the fluorophore or have overlapping absorbance/emission with the fluorophore will lead to false positive/negative results.

Our studies have shown that reducing reagents such as dithiothreitol (DTT) or glutathione are essential in the FRET

enzymatic buffer to rule out promiscuous compounds that have non-specific inhibition against cysteine proteases. Our recent studies of validation and invalidation of reported M^{pro} and PL^{pro} inhibitors demonstrated that the FRET IC₅₀ values obtained in the absence of reducing reagent DTT had poor correlation with the antiviral activity.^{64–66} We therefore urge the scientific community to be cautious in interpreting the PL^{pro} assay IC₅₀ values obtained in the absence of reducing reagent.

Several binding assays are also commonly used to determine the binding affinity between inhibitors and the PL^{pro}: the thermal shift assay,⁵⁴ the surface plasma resonance (SPR) assay,⁶⁷ and isothermal titration calorimetry (ITC).⁶⁸ The thermal shift assay measures protein stability, and ligand binding typically leads to an increase of the melting temperature *T*_m. Nevertheless, a decrease in protein stability is also observed for certain ligand–protein interactions. Compared to the thermal shift assay, SPR is more quantitative, and binding kinetics *k*_{on}, *k*_{off} and *K*_D can be derived from the binding curves. ITC can determine the thermodynamic binding parameters Δ*G*, Δ*H*, and Δ*S* in a single experiment without a need to modify the protein. To gain a molecular-level understanding of the PL^{pro}–inhibitor interactions, a co-crystal structure needs to be solved.

It is expected that the cell-free enzymatic assay or binding assay results can be used to faithfully predict the cellular antiviral activity. However, SARS-CoV-2 is a biological safety level 3 (BSL-3) pathogen, which limits the number of compounds that can be tested in the antiviral assay, given the paucity of the resources. In this regard, there is a need for a cell-based protease assay to help predict the antiviral activity at the BSL-1/2 setting. The cell-based protease assay not only reveals intracellular target engagement but also can rule out compounds that are cell-membrane-impermeable or cytotoxic. The FlipGFP and Protease-Glo luciferase assays are two representative cell-based protease assays that have been applied for the screening and validation of SARS-CoV-2 PL^{pro} inhibitors.^{54,69} In the FlipGFP assay, cells are transfected with two plasmids, one expressing the PL^{pro} and another expressing the GFP reporter (Figure 4C).^{70–72} The reporter plasmid encodes three proteins: the

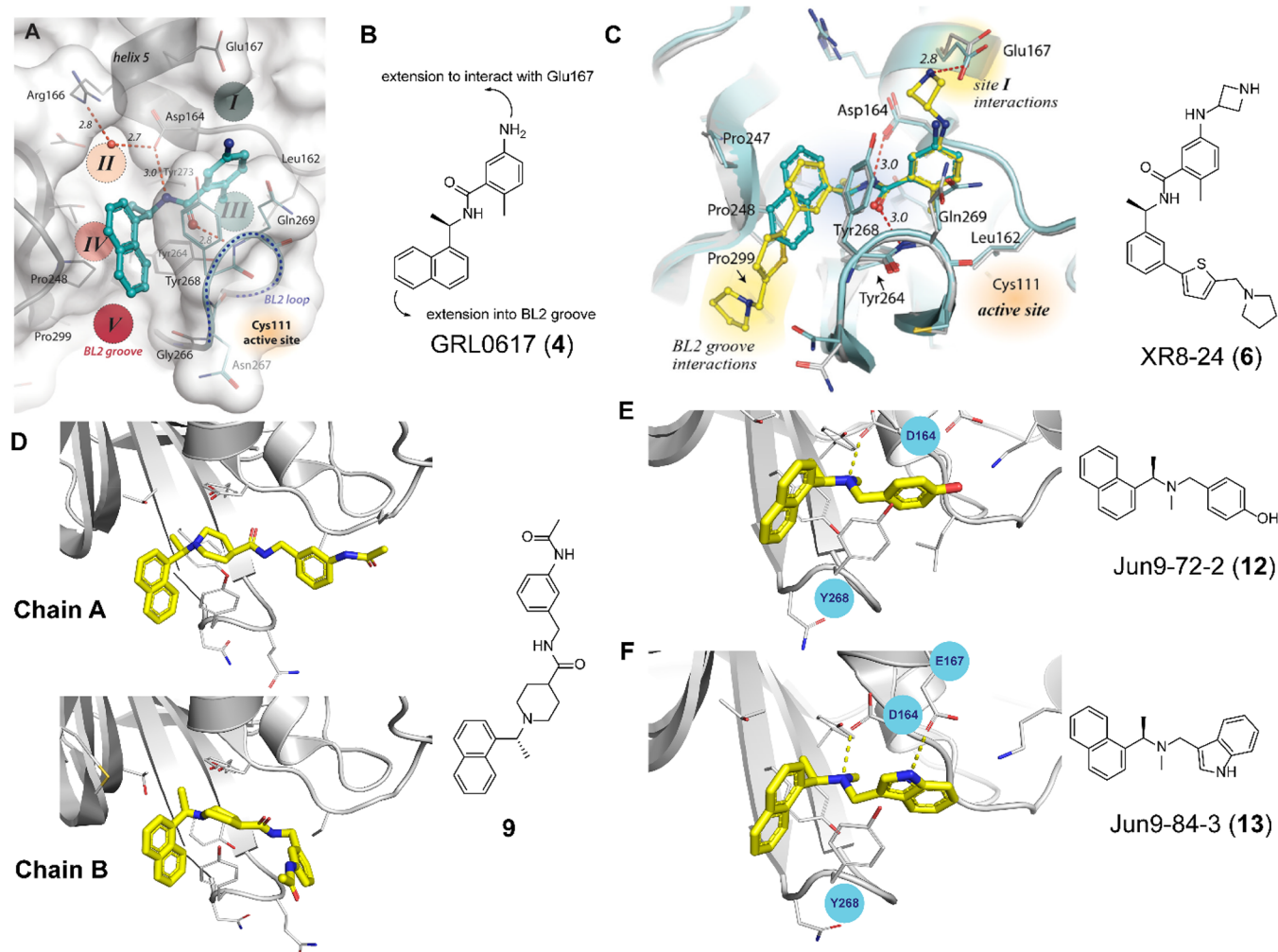


Figure 5. GRL0617-based SARS-CoV-2 PL^{pro} inhibitors. (A) X-ray crystal structure of SARS-CoV-2 PL^{pro} with GRL0617 (4) (PDB: 7JRN). (B) Design hypothesis for the 2-phenylthiophene series of PL^{pro} inhibitors based on GRL0617 (4). (C) X-ray crystal structure of SARS-CoV-2 PL^{pro} with compound XR8-24 (6) (PDB: 7LBS). (D) X-ray crystal structure of SARS-CoV-2 PL^{pro} with compound 9 (PDB: 7E35). (E) X-ray crystal structure of SARS-CoV-2 PL^{pro} with Jun9-72-2 (12) (PDB: 7SDR). (F) X-ray crystal structure of SARS-CoV-2 PL^{pro} with Jun9-84-3 (13) (PDB: 7SQE). Panels A and C were adapted with permission from ref 67. Copyright 2022 American Chemical Society.

GFP β 1–9 template, the β 10–11 fragment, and the mCherry. The β 10–11 fragment is restrained in the parallel orientation through the K5/E5 coiled coil and therefore cannot associate with the β 1–9 template. Upon cleavage of the PL^{pro} substrate linker, β 10 and β 11 become antiparallel and can associate with the β 1–9 template, leading to the restoration of the GFP signal. mCherry serves as an internal control to normalize the transfection efficiency. As such, the GFP/mCherry ratio correlates to the enzymatic activity of PL^{pro}. Results from us as well as others have shown that the FlipGFP assay is a valuable assay in characterizing the cellular M^{pro} and PL^{pro} inhibition without the need of the infectious SARS-CoV-2 virus.^{54,64,69,70,72,73} A positive correlation between the FlipGFP IC₅₀ values and the antiviral EC₅₀ values was observed for the PL^{pro} inhibitors,⁵⁴ suggesting the FlipGFP assay can be used as a surrogate assay to prioritize lead compounds for antiviral testing.

The Protease-Glo luciferase assay is designed in an analogous way as the FlipGFP assay, in which the luciferase activity depends on cleavage of the substrate linker by the protease.⁶⁴ Specifically, the firefly luciferase is engineered with a protease substrate cleavage sequence (Figure 4D). Before cleavage, firefly luciferase is in the permuted circular inactive conformation.

Upon protease cleavage, a conformational change leads to association of the two domains and restoration of the luciferase activity. The Protease-Glo luciferase assay can be performed either in live cells or in cell lysates.^{69,74,75} As the readout is luminescence, the Protease-Glo luciferase assay can help rule out compounds that have fluorescence interference properties. Other cell-based assays, including the GFP ER translocation assay, the bioluminescence resonance energy transfer (BRET) assay, and the cell cytotoxicity assay, can be similarly engineered for PL^{pro}.^{75–77}

3. SARS-CoV-2 PL^{pro} INHIBITORS

We group SARS-CoV-2 PL^{pro} inhibitors into non-covalent inhibitors and covalent inhibitors. The non-covalent inhibitors are further divided into GRL0617 (4) analogues and non-GRL0617 inhibitors (Table 1).

3.1. Non-covalent SARS-CoV-2 PL^{pro} Inhibitors.

3.1.1. GRL0617 Analogues. The naphthalene-containing GRL0617 (4) was a well-characterized SARS-CoV PL^{pro} inhibitor. It was originally developed through lead optimization based on a high-throughput screening (HTS) hit.⁶² Several follow-up studies have been conducted with the aim of

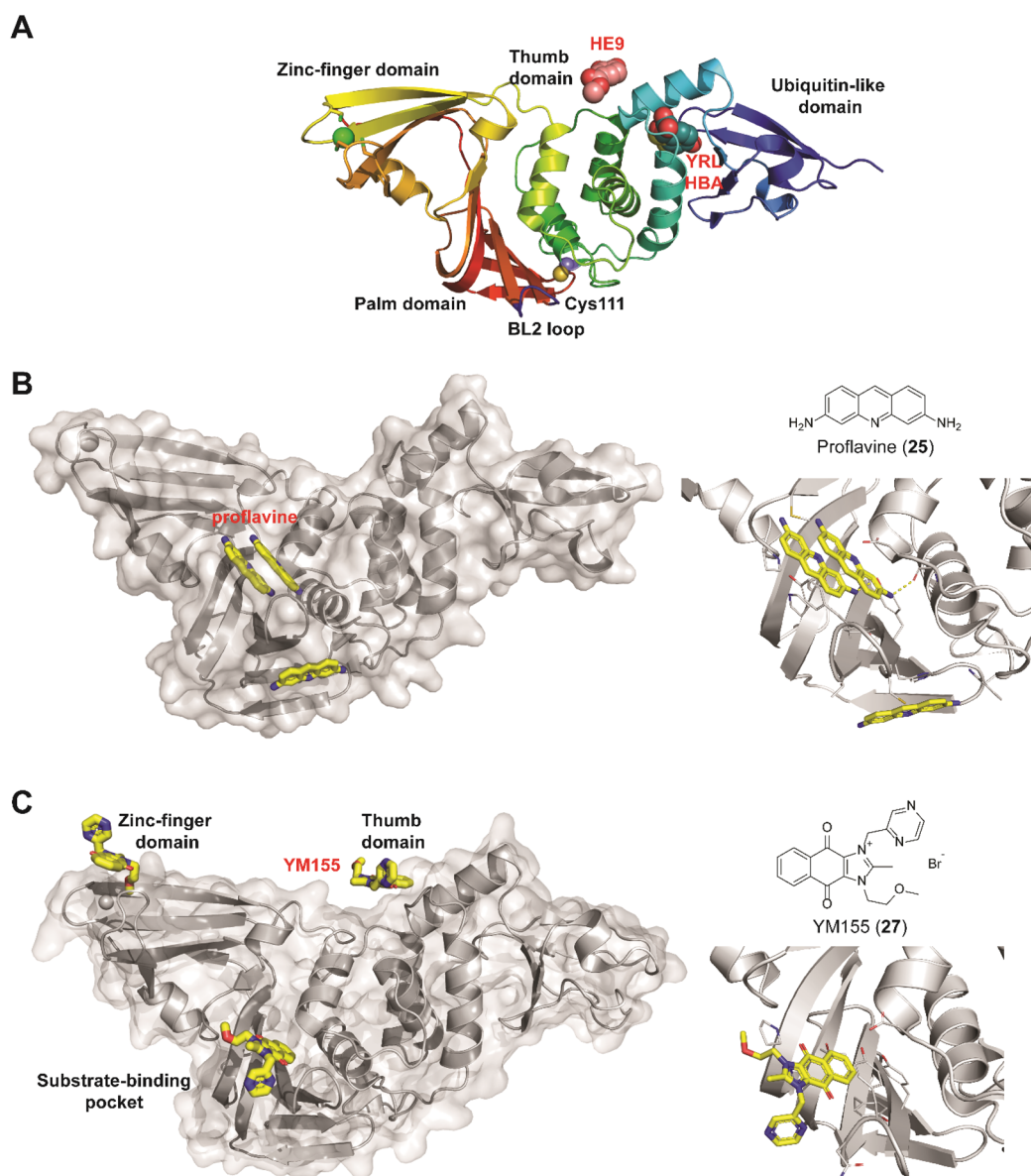


Figure 6. Non-covalent SARS-CoV-2 PL^{pro} inhibitors that do not share structural similarity with GRL0617 (4). (A) X-ray crystal structures of SARS-CoV-2 PL^{pro} in complex with fragments HE9 (20), YRL (21), and HBA (22). (B) X-ray crystal structure of SARS-CoV-2 PL^{pro} in complex with proflavine (25), showing three molecules binding near the BL2 loop (PDB: 7NT4). Two molecules stack on top of each other and fit in the GRL0617 (4) binding pocket, and a third molecule binds at the backside of the BL2 loop. (C) X-ray crystal structures of SARS-CoV-2 PL^{pro} in complex with YM155 (27) (PDB: 7D7L). YM155 (27) binds three different sites located at the zinc-finger domain, thumb domain, and the substrate-binding pocket. Detailed interactions between YM155 and the BL2 loop region residues are shown on the right side.

improving the potency of enzymatic inhibition and antiviral activity as well as pharmacokinetic (PK) properties. However, no significant improvement has been achieved.^{60,61} As the SARS-CoV-2 PL^{pro} is 83% identical and 90% similar to SARS-CoV PL^{pro}, GRL0617 (4) became a top candidate as the SARS-CoV-2 PL^{pro} inhibitor. Several groups independently showed the potent inhibition of SARS-CoV-2 PL^{pro} by GRL0617 (4).^{45,53,54,68,78} However, the moderate to weak antiviral activity of GRL0617 (4) prevents it from advancing to animal model studies.^{54,67} Since the beginning of the COVID-19 pandemic, encouraging progress has been made in redesigning GRL0617 analogues as potent SARS-CoV-2 PL^{pro} inhibitors. The X-ray crystal structure of SARS-CoV-2 PL^{pro} in complex with GRL0617 (4) has also been solved by multiple

groups,^{53,54,56,57,78} paving the way for structure-based lead optimization.

A recent elegant structure-based drug design led to the discovery of potent PL^{pro} inhibitors with favorable PK properties.⁶⁷ One of the major contributions of this study is the conversion of naphthalene to 2-phenylthiophene, which leads to improved PK properties. In addition, the thiophene substitution extends further into the BL2 groove (Figure 5A), and when it was coupled with additional substitutions on the aniline amine to engage interaction with Glu167 (Figure 5B,C), multiple nanomolar PL^{pro} inhibitors have been identified. Among the more than 100 analogues tested, compounds ZN-3-80 (5), XR8-24 (6), and XR8-23 (7) were the most potent ones, with IC₅₀ values of 0.59, 0.56, and 0.39 μ M, respectively (Table 1). Compounds 6 and 7 also showed a significantly

improved antiviral activity against SARS-CoV-2 in A549-hACE2 cells, with EC₅₀ values of 1.2 and 1.4 μM, respectively. In comparison, GRL0617 (**4**) was not active in the virus yield reduction antiviral assay (EC₅₀ > 20 μM). The complex structure with compound XR8-24 (**6**) (PDB: 7LBS) revealed several key hydrogen bonds/electrostatic interactions, including the water-mediated hydrogen bonds between the pyrrolidine NH⁺ and the main-chain carbonyl oxygen of Tyr264 (not shown), the electrostatic interaction between the NH²⁺ from the azetidine ring and side-chain carboxylate from Glu167 (Figure 5C), and the hydrogen bond between the amide NH from compound XR8-24 (**6**) with the Asp164 side-chain carboxylate. When dosed in male C57BL/6 mice at 50 mg/kg by intraperitoneal injection (i.p.), compounds XR8-23 (**7**) and XR8-24 (**6**) reached C_{max} = 6130 and 6403 ng/mL, respectively, indicating favorable *in vivo* bioavailability. Further optimization might lead to candidates that are suitable for *in vivo* antiviral efficacy studies.

In another study, Shan et al. reported the structure-based design of SARS-CoV-2 PL^{pro} inhibitors based on the GRL0617 scaffold.⁷⁹ The most potent lead compound, **8**, inhibited PL^{pro} and SARS-CoV-2 viral replication, with IC₅₀ = 0.44 μM and EC₅₀ = 0.18 μM, respectively (Table 1). The K_d was 2.60 μM for compound **8** in the SPR assay, compared to K_d = 10.79 μM for GRL0617 (**4**). In the counter screening against 10 deubiquitinases (DUBs) or DUB-like proteases, compound **8** was highly selective toward PL^{pro} and did not show significant inhibition toward a panel of host DUBs and DUB-like proteases. The X-ray crystal structure of PL^{pro} with an analogue, **9**, showed that compound **9** binds to PL^{pro} in a similar mode as GRL0617 (**4**) (Figure 5D). It is noted that compound **9** adapts different binding poses in the two monomers (Figure 5D).

Our group recently conducted a HTS against SARS-CoV-2 PL^{pro} using the FRET-based enzymatic assay.⁵⁴ Two closely related compounds, Jun9-13-7 (**10**) and Jun9-13-9 (**11**), were identified as potent hits, with IC₅₀ values of 7.9 and 6.67 μM, respectively (Table 1). Subsequent lead optimization led to the discovery of several compounds with IC₅₀ values in the submicromolar range, including Jun9-72-2 (**12**) (IC₅₀ = 0.67 ± 0.08 μM) and Jun9-84-3 (**13**) (IC₅₀ = 0.67 ± 0.14 μM). In the cell-based FlipGFP reporter assay, Jun9-72-2 (**12**) and Jun9-84-3 (**13**) showed dose-dependent inhibition, with EC₅₀ values of 7.93 and 17.07 μM, respectively, suggesting both compounds are cell-membrane-permeable and can inhibit the intracellular protease activity of PL^{pro}. In agreement, both compounds had potent antiviral activity against SARS-CoV-2 in Vero E6 and Caco2-hACE2 cells (Table 1). Significantly, there is a positive correlation between the FlipGFP assay results and the antiviral assay results, validating the FlipGFP as a surrogate assay for the prediction of the antiviral activity of PL^{pro} inhibitors.⁵⁴ In the X-ray crystal structure of PL^{pro} with Jun9-72-2 (**12**) (PDB: 7SDR), the tertiary NH⁺ in the linker electrostatically interacts with the Asp164 carboxylate group (Figure 5E). The X-ray crystal structure of PL^{pro} with Jun9-84-3 (**13**) (PDB: 7SQE) revealed an additional hydrogen bond between the indole NH and the Glu167 side-chain carboxylate (Figure 5F).

Additional GRL0617 analogues, **14–19**, have been reported as SARS-CoV-2 PL^{pro} inhibitors (Table 1);^{52,53,68} however, no significant improvement has been made.

3.1.2. Non-GRL0617 Inhibitors. Three phenolic compounds—methyl 3,4-dihydroxybenzoate (HE9, **20**), 4-(2-hydroxyethyl)phenol (YRL, **21**), and 4-hydroxybenzaldehyde (HBA, **22**)—were identified as allosteric SARS-CoV-2 PL^{pro}

inhibitors through a high-throughput X-ray crystallization.⁵⁵ The screened library contains 500 compounds from the International Center for Chemical and Biological Sciences (ICCBS) Molecular Bank. Interestingly, HE9 (**20**), YRL (**21**), and HBA (**22**) all bind to the ISG15/Ub-S2 binding site of PL^{pro} (Figure 6A), an allosteric binding pocket that has not been explored for drug design. The allosteric binding site is located about 30 Å away from the active-site residue Cys111. The superimposition structures of PL^{pro} + inhibitors and PL^{pro} + ISG15 indicate that these compounds might compete with ISG15 for the same binding site. As expected, all three compounds inhibited the deISGylating activity of PL^{pro}, with IC₅₀ values of 3.76 ± 1.13 μM (**20**), 6.68 ± 1.20 μM (**21**), and 3.99 ± 1.33 μM (**22**). However, it remains unknown whether these compounds can inhibit the hydrolysis of viral polyprotein by PL^{pro}. HE9 (**20**) and YRL (**21**) inhibited SARS-CoV-2 replication in Vero E6 cells in the qRT-PCR assay, with EC₅₀ values of 0.13 and 1 μM, respectively. However, the antiviral assay results for HBA (**22**) were not conclusive. In the cytopathic effect (CPE) assay, HE9 (**20**) had an EC₅₀ of 10.37 μM. In contrast, YRL (**21**) failed to show inhibition in the CPE assay. The discrepancy of antiviral activity in different assays suggests further validation is needed. Furthermore, these results raise the question of whether inhibiting the deISGylation activity of PL^{pro} alone is sufficient for the inhibition of viral replication.

A drug repurposing screening by Napolitano et al. identified acriflavine (**23**) as a potent inhibitor of SARS-CoV-2 PL^{pro} with *in vivo* antiviral efficacy.⁸² Acriflavine (**23**) is a mixture of tryptaflavine (**24**) and proflavine (**25**).⁸² Acriflavine (**23**) inhibited PL^{pro} with IC₅₀ values of 1.66 and 1.46 μM when RLRGG-AMC and ISG15-AMC were used as substrates, respectively (Table 1). Acriflavine (**23**) also inhibited the deubiquitylating activity of PL^{pro} in gel-based assay, thus ruling out the potential fluorescence interference effect of acriflavine (**23**). In addition, acriflavine (**23**) did not inhibit M^{pro}. The X-ray crystal structure of PL^{pro} with proflavine (**25**) was determined (PDB: 7NT4), revealing that two molecules of proflavine (**25**) bind to the S3–S5 pockets of PL^{pro} simultaneously (Figure 6B). The BL2 loop folds inward toward the substrate-recognition cleft, similar to the binding mode of GRL0617 (**4**). A third proflavine (**25**) molecule is located at the surface of the protein on the opposite side of the BL2 loop. Acriflavine (**23**) inhibited SARS-CoV-2 replication in A549-ACE2 and Vero cells, with EC₅₀ values of 86 and 64 nM, respectively. However, the selectivity index was low (A549-ACE2 SI = 36; Vero SI = 53). The antiviral activity was further confirmed in human airway epithelial (HAE) cells. Acriflavine (**23**) also showed potent inhibition against MERS-CoV (IC₅₀ = 21 nM, SI = 162) and HCoV-OC43 (IC₅₀ = 105 nM, SI = 27) but not the alphacoronaviruses, including feline infectious peritonitis virus (FIPV) and HCoV-NL63. In the *in vivo* SARS-CoV-2 infection model with K18-ACE2 mice, acriflavine (**23**) treatment by either i.p. or intramuscular (i.m.) injection significantly lowered the viral titers in the brain and the lung.

6-Thioguanine (6-TG, **26**) was previously reported as an inhibitor for SARS-CoV and MERS-CoV;^{92,93} therefore, it was hypothesized that it might also inhibit the SARS-CoV-2 PL^{pro}. Swaim et al. recently demonstrated that 6-TG (**26**) is a potent inhibitor for SARS-CoV-2 in Vero E6 cells, with an EC₅₀ of 2.13 μM (Table 1).⁹⁴ Next, to confirm the intracellular inhibition of PL^{pro} by 6-TG (**26**), a TAP-tagged pp1a protein consisting of nsp1, 2, and 3 was expressed. As expected, TAP-nsp1 was the

major product due to the self-cleavage of the pp1a polyprotein by PL^{Pro}. Treatment with 6-TG (26) led to dose-dependent inhibition of the cleavage, with an IC₅₀ of approximately 0.5 μM. In addition, 6-TG (26) showed potent inhibition of the deISGylation activity of PL^{Pro} in HEK293T cells. No *in vitro* enzymatic assay was performed. In addition, it was proposed that 6-TG (26) might have a secondary mechanism of action by inhibiting the viral RNA synthesis. Nonetheless, in our recently hit validation study, 6-TG (26) did not show inhibition against SARS-CoV-2 PL^{Pro} in the enzymatic assay (IC₅₀ > 50 μM), had no binding to PL^{Pro} in the thermal shift assay, and did not inhibit the intracellular PL^{Pro} activity in the FlipGFP assay.⁶⁹ Therefore, the antiviral activity of 6-TG (26) may not arise from inhibiting the PL^{Pro}.

Through screening a library of 6000 compounds using the FRET-based enzymatic assay with the Arg-Leu-Arg-Gly-Gly-AMC substrate, Zhao et al. identified YM155 (27) (IC₅₀ = 2.47 ± 0.46 μM), cryptotanshinone (28) (IC₅₀ = 5.63 ± 1.45 μM), tanshinone I (29) (IC₅₀ = 2.21 ± 0.10 μM), and GRL0617 (4) (IC₅₀ = 1.39 ± 0.26 μM) as SARS-CoV-2 PL^{Pro} inhibitors (Table 1).⁸⁰ All four compounds displayed potent antiviral activity against SARS-CoV-2 in Vero E6 cells, with the most potent compound being YM155 (27) (EC₅₀ = 0.17 ± 0.02 μM, CC₅₀ ≈ 400 μM). The structure of PL^{Pro} in complex with YM155 (27) was solved by crystal soaking (PDB: 7D7L). Unexpectedly, YM155 (27) was found in three different binding sites: the orthosteric site, the thumb domain, and the zinc-finger domain (Figure 6C). The binding at the thumb domain is expected to inhibit the binding between PL^{Pro} and ISG15. A conformational change was observed at the zinc-finger domain upon YM155 (27) binding, but the physiological relevance of this binding mode has not been validated.

Similarly, cryptotanshinone (28) (IC₅₀ = 1.34 μM) and two other analogues, dihydrotanshinone I (30) (IC₅₀ = 0.59 μM) and tanshinone IIA (31) (IC₅₀ = 1.57 μM), were shown as potent SARS-CoV-2 PL^{Pro} inhibitors through a HTS (Table 1).⁸¹ In addition, four additional compounds, PKK1/Akt/Flt dual pathway inhibitor (32) (IC₅₀ = 0.26 μM), Ro 08-2750 (33) (IC₅₀ = 0.53 μM), Cdk4 inhibitor III (34) (IC₅₀ = 0.39 μM), and β-lapachone (35) (IC₅₀ = 0.61 μM), were also identified as potent PL^{Pro} inhibitors (Table 1). Dihydrotanshinone I (30) inhibited SARS-CoV-2 with an EC₅₀ of 8.15 μM. Unexpectedly, cryptotanshinone (28) and tanshinone IIA (31) had no antiviral activity (EC₅₀ > 200 μM), despite their potent enzymatic inhibition. The antiviral result of cryptotanshinone (28) is also in controversy with the previous study, which showed that cryptotanshinone (28) is a potent antiviral with an EC₅₀ of 0.7 μM.⁸⁰ Further validation is needed to test the antiviral activity of cryptotanshinone (28) against SARS-CoV-2 in multiple cell lines.

Xu et al. recently reported the discovery of tanshinone IIA sulfonate (36) and chloroxine (37) as SARS-CoV-2 PL^{Pro} inhibitors from a drug-repurposing screening.⁸³ Tanshinone IIA sulfonate (36) was identified in the fluorogenic assay using the ALKGG-AMC substrate, with an IC₅₀ of 1.65 μM (Table 1). Chloroxine (37) was discovered in the fluorescence polarization-based assay using the fluorescein 5-isothiocyanate (FITC)-labeled ISG15, with an IC₅₀ of 7.24 μM. Tanshinone IIA sulfonate (36) and chloroxine (37) also showed binding to PL^{Pro} in the biolayer interferometry and thermal shift assays. The antiviral activity against SARS-CoV-2 was not reported.

We performed hit validations for YM155 (27), cryptotanshinone (28), tanshinone I (29), dihydrotanshinone I (30), and

tanshinone IIA (31).⁶⁹ Our study found that YM155 (27) (IC₅₀ = 20.13 μM), cryptotanshinone (28) (IC₅₀ = 52.24 μM), tanshinone I (29) (IC₅₀ = 18.58 μM), dihydrotanshinone I (30) (IC₅₀ = 33.01 μM), and tanshinone IIA (31) (IC₅₀ = 15.30 μM) had much higher IC₅₀ values against SARS-CoV-2 PL^{Pro} in the FRET assay compared to the previous reports. The intracellular PL^{Pro} inhibition by YM155 (27) and cryptotanshinone (28) in the FlipGFP assay was not conclusive due to cell cytotoxicity, while tanshinone I (29), dihydrotanshinone I (30), and tanshinone IIA (31) had no intracellular PL^{Pro} inhibition at non-toxic concentrations. Collectively, our results suggest that YM155 (27), cryptotanshinone (28), tanshinone I (29), dihydrotanshinone I (30), and tanshinone IIA (31) are weak PL^{Pro} inhibitors and tanshinone I (29), dihydrotanshinone I (30), and tanshinone IIA (31) lack intracellular target engagement.

In agreement with our results, Brewitz et al. applied a mass spectrometry assay to monitor PL^{Pro}-mediated cleavage of the nsp2/3 substrate.⁹⁵ Among the list of compounds tested, YM155 (27), tanshinone I (29), and tanshinone IIA sulfonate sodium (36) were not active (IC₅₀ > 50 μM), while cryptotanshinone (28) showed moderate activity, with an IC₅₀ of 19.4 μM.

Through virtual screening of a library of naphthoquinoidal compounds followed by enzymatic assay validation, Santos et al. identified three compounds, 38, 39, and 40, as potent SARS-CoV-2 PL^{Pro} inhibitors, with IC₅₀ values of 1.7, 2.2, and 3.1 μM, respectively (Table 1).⁸⁴ Among the three hits, compound 40 had moderate inhibition against M^{Pro}, with an IC₅₀ of 66 μM; therefore, it was considered as a dual inhibitor for further optimization. Molecular dynamics (MD) simulations predicted that compound 39 binds non-covalently to the S3 and S4 subsites in PL^{Pro}. However, the detailed mechanism of action remains to be characterized. When tested in the antiviral assay against SARS-CoV-2 in two different cell lines, Vero E6 and HeLa-ACE2, none of the identified M^{Pro} and PL^{Pro} inhibitors had antiviral activity, suggesting these naphthoquinoidal compounds might have off-target effects. It is noted that no reducing agent such as DTT was added in the M^{Pro} enzymatic assay; however, 0.1 mM DTT was included in the PL^{Pro} assay. Therefore, the observed PL^{Pro} inhibition might not be due to non-specific modification of the PL^{Pro} C111 residue. Further validation studies are warranted to confirm their enzymatic inhibition.

Cho et al. reported SJB2-043 (41) as a SARS-CoV-2 PL^{Pro} inhibitor, with an apparent IC₅₀ of 0.56 μM.⁸⁵ However, no complete inhibition was achieved at high drug concentration. Therefore, it remains to be validated whether SJB2-043 (41) is a specific PL^{Pro} inhibitor.

Commercial mouth rinses are known to inactivate SARS-CoV-2,^{96,97} but the detailed mechanism remains elusive. Lewis et al. tested the active ingredients of mouth rinses against the SARS-CoV-2 M^{Pro} and PL^{Pro}.⁸⁶ Although none of the compounds were active against M^{Pro}, two compounds, aloin A (42) and aloin B (43), inhibited PL^{Pro}, with IC₅₀ values of 13.16 and 16.08 μM, respectively, in the enzymatic assay. Aloin A (42) and B (43) also inhibited the deubiquitinating activity of PL^{Pro}, with IC₅₀ values of 15.68 and 17.51 μM. MD simulations suggest that aloin A (42) and B (43) bind to the GRL0617 (4) binding site and mainly interact with Glu167, Tyr268, and Glu269.

3.2. Specific Covalent PL^{Pro} Inhibitors. The cleavage of PL^{Pro} substrate occurs after the second glycine in the Leu-X-Gly-Gly sequence.⁵⁷ As a result, the binding pockets for the S2 and

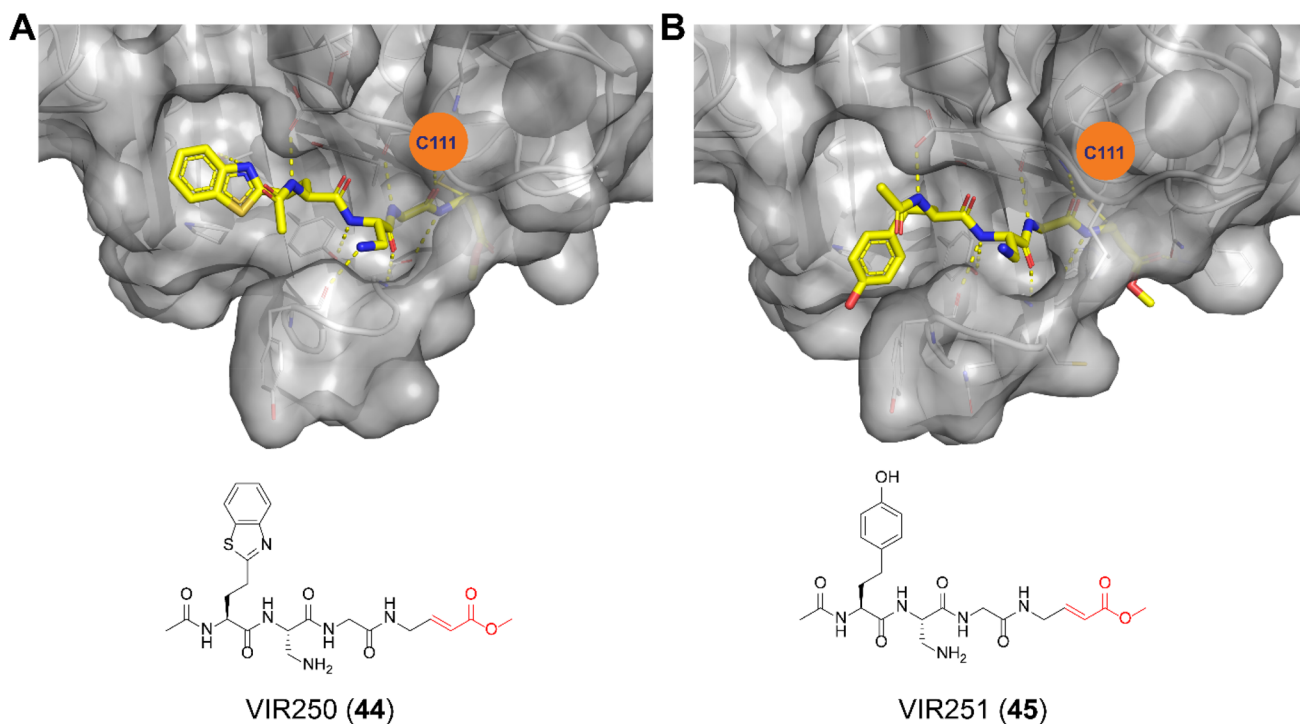


Figure 7. X-ray crystal structures of SARS-CoV-2 PL^{pro} in complex with peptidomimetic covalent inhibitors VIR250 (**44**) (PDB: 6WUU) (A) and VIR251 (**45**) (PDB: 6WX4) (B).

S1 subsites are absent, which leaves the S4 and S3 subsites for inhibitor binding. Accordingly, to develop a covalent inhibitor to react with the catalytic C111, a linker is needed to conjugate the S4/S3 pocket binder with a reactive warhead.^{53,57}

A positional scanning was conducted to identify the optimal substrate of SARS-CoV-2 PL^{pro}.⁵⁷ A total of 19 natural and 109 non-proteinogenic amino acids were screened at each position. It was found that the P2 and P4 positions have high preference for glycine and hydrophobic residues, respectively, while the P3 position can tolerate both charged residues, including Phe(guan), Dap, Dab, Arg, Lys, Orn, and hArg, and hydrophobic residues, including hTyr, Phe(F5), Cha, Met, Met(O), Met(O)₂, and D-hPhe. Leveraging this information, two covalent inhibitors, VIR250 (**44**) (Ac-Abu(Bth)-Dap-Gly-Gly-VME) and VIR251 (**45**) (Ac-hTyr-Dap-Gly-Gly-VME), were designed by incorporating the optimal P3 and P4 substitutions with the vinyl methyl ester (VME)-reactive warhead (Table 1). VIR250 (**44**) and VIR251 (**45**) showed dose-dependent inhibition against both SARS-CoV-2 and SARS-CoV PL^{pro}s; however, the IC₅₀ values were not quantified. The X-ray crystal structures of SARS-CoV-2 PL^{pro} in complex with VIR250 (**44**) (PDB: 6WUU) and VIR251 (**45**) (PDB: 6WX4) were solved (Figure 7), revealing covalent thioether linkage of the C111 thiol and the β carbon of the vinyl group. Although no antiviral assay results were reported, this is an elegant rational design that led to the first covalent SARS-CoV-2 PL^{pro} inhibitors.

Sanders et al. recently reported the rational design of the first-in-class drug-like covalent SARS-CoV-2 PL^{pro} inhibitors.⁸⁷ An *N,N'*-diacetylhydrazine linker was designed as a mimetic of the Gly-Gly to conjugate the GRL0617 methyl group with different reactive warheads. A series of commonly used cysteine-reactive warheads, including fumarate methyl ester, chloroacetamide, propiolamide, cyanoacetamide, and α -cyanoacrylamide, have been exploited. Among the designed covalent PL^{pro} inhibitors, compounds **46** and **47** with the fumarate methyl ester, and

compound **48** with the propiolamide, showed significantly improved potency, with IC₅₀ values of 0.094, 0.230, and 0.098 μ M, respectively (Table 1). Compound **49**, with the chloroacetamide, and compound **50**, with the cyanoacetamide, were less active, with IC₅₀ values of 5.4 and 8.0 μ M, respectively. In contrast, compound **51**, with the α -cyanoacrylamide, was not active (IC₅₀ > 200 μ M). As expected, covalent protein adducts with inhibitors were observed for compounds **46**–**50** in electrospray ionization (ESI) mass spectrometry. The X-ray crystal structure of PL^{pro} with compound **46** was solved at 3.10 Å resolution (PDB: not released), showing a covalent adduct between the C111 thiol and the C1 of compound **46**. The *N,N'*-diacetylhydrazine linker forms four hydrogen bonds with Gly163 and Gly271, highlighting the importance of this rationally designed linker. In SARS-CoV-2-infected Vero E6 cells, compound **46** had an EC₅₀ of 1.1 μ M, which is comparable to the potency of remdesivir (EC₅₀ = 0.74 μ M). Surprisingly, compound **47** had insignificant cytoprotective effects, despite its potent enzymatic inhibition. Compound **48** was cytotoxic; therefore, its antiviral activity was not conclusive. Similar to GRL0617 (**4**), compound **46** also inhibited the deubiquitinating and the deISGylating activities, with IC₅₀ values of 76 and 39 nM, respectively. Selectivity screening against a panel of DUBs showed that compound **46** is highly selective, and no inhibition was observed up to 30 μ M. *In vitro* PK profiling showed that compound **46** is stable in human liver S9 and microsomes, with *T*_{1/2} = 60 and 50 min, respectively. This study represents the first rational design of drug-like covalent PL^{pro} inhibitors with potent antiviral activity, and the X-ray crystal structures are invaluable in guiding the lead optimization.

Liu et al. reported the design of peptide–drug conjugates (PDCs) as covalent inhibitors of SARS-CoV-2 PL^{pro}.⁸⁸ The PDCs consist of GRL0617 and cyclic sulfonium-containing peptides derived from PL^{pro} substrate Leu-Arg-Gly-Gly (Table 1). The sulfonium serves as a warhead and is designed to react

with the C111. Among the examined PDCs, EM-C (52) and EC-M (53) were the most potent against SARS-CoV-2 PL^{pro}, with IC₅₀ values of 7.40 ± 0.37 and 8.63 ± 0.55 μM, respectively (Table 1). Both conjugates were cell-membrane-permeable and inhibited the deISGylating activity of PL^{pro}. In-gel digestion of the PL^{pro} + PDC mixture followed by MS/MS analysis confirmed that C111 is the enriched conjugation site. No antiviral assay results were presented. Although the results presented convincingly demonstrated the covalent labeling of PL^{pro} C111, their binding mode remains unknown. The EC-M (52) and EM-C (53) PDCs contain the GRL0617 and the Leu-Arg dipeptide sequence, both of which are S3 and S4 subsite binders. It is not clear why the design contains duplicate binding elements. The X-ray crystal structure might solve the puzzle.

A tryptophan-containing dipeptide, compound 54, was recently reported as a dual inhibitor of SARS-CoV-2 M^{pro} and PL^{pro}.⁸⁹ Compound 54 inhibited M^{pro} and PL^{pro} with IC₅₀ values of 1.72 and 0.67 μM, respectively, while it had no binding to the viral spike protein (K_D > 25 μM). In the antiviral assay, compound 54 inhibited two SARS-CoV-2 clinical isolates, UC-1074 and UC-1075, with EC₅₀ values of 0.32 and 1.37 μM, respectively. Given the lack of structural similarities between M^{pro} and PL^{pro}, coupled with the high reactivity of the α-chloroacetamide warhead in 54, it remains to be investigated whether the inhibition of M^{pro} and PL^{pro} by compound 54 is specific. Nevertheless, the potent antiviral activity of compound 54 is encouraging, which warrants further optimization.

3.3. Non-specific Covalent PL^{pro} Inhibitors. **3.3.1. Ebselen Analogues.** Given the broad-spectrum antiviral activity of ebselen against several viruses, Weglarz-Tomczak et al. explored ebselen and its analogues as SARS-CoV-2 PL^{pro} inhibitors.⁹⁰ Ebselen (55) inhibited PL^{pro} with an IC₅₀ of 2.02 ± 1.02 μM, and dialysis experiment showed that no enzymatic activity was recovered, suggesting irreversible inhibition. Subsequently, a library of analogues was designed, among which two ebselen derivatives, 56 (IC₅₀ = 236 ± 107 nM) and 57 (IC₅₀ = 256 ± 35 nM), and two diselenide orthologs, 58 (IC₅₀ = 339 ± 109 nM) and 59 (IC₅₀ = 263 ± 121 nM), had improved enzymatic inhibition against SARS-CoV-2 PL^{pro} compared to ebselen (55) (IC₅₀ = 2.02 ± 1.02 μM) (Table 1). In this study, 2 mM DTT was added in the enzymatic assay buffer. However, our previous studies showed that ebselen (55) only inhibited SARS-CoV-2 PL^{pro} in the absence of DTT but not with DTT.⁶⁵ This discrepancy needs to be further validated.

In another study, a similar strategy has been exploited for the development of dual inhibitors targeting both SARS-CoV-2 M^{pro} and PL^{pro} based on the ebselen scaffold.⁹¹ Among the 23 ebselen analogs, seven showed dual inhibition with the M^{pro} IC₅₀ values in the nanomolar range and the PL^{pro} IC₅₀ values in the single digit to submicromolar range (60–66, Table 1). No reducing reagent was added in either the M^{pro} or the PL^{pro} enzymatic assay. The antiviral activity of the potent hits was not reported. Nonetheless, ebselen (55) was previously reported to inhibit SARS-CoV-2 replication, with an EC₅₀ value of 4.67 μM in the plaque assay, albeit the proposed mechanism of action is through M^{pro} inhibition.⁹⁸

The inconsistent PL^{pro} enzymatic inhibitory activity of ebselen (55) and its analogues from several groups, coupled with their antiviral activity against SARS-CoV-2, suggest that further characterizations are needed to confirm their cellular PL^{pro} target engagement and additional targets that might contribute to the antiviral activity.

3.3.2. Zinc Ejector. PL^{pro} contains a zinc-binding domain (ZBD) in which the zinc ion is coordinated by four conserved cysteine residues: Cys₁₈₉, Cys₁₉₂, Cys₂₂₄, and Cys₂₂₆. The ZBD is essential for the structural integrity and hence the enzymatic activity of PL^{pro}. As such, the cysteine-rich ZBD was also proposed as a putative drug target.⁹⁹

Disulfiram (67) and ebselen (55), together with 5,5'-dithiobis(2-nitrobenzoic acid) (DTNB, 68), 2,2'-dithiodipyridine (69), and 2,2'-dithiobis(benzothiazole) (70), were found to eject zinc from PL^{pro}, as shown by the increase in fluorescence emission signal from the zinc-specific fluorophore, FluoZin-3.¹⁰⁰ The matrix-assisted laser desorption/ionization time-of-flight (MALDI-TOF) mass spectrum further confirmed formation of the covalent adduct between disulfiram and ebselen with PL^{pro} and nsp10. The LC-MS/MS experiment mapped the ebselen and disulfiram conjugation sites to C189 and C192, both of which are involved in zinc chelation in the ZBD of PL^{pro}. In the FRET-based enzymatic assay, disulfiram (67) and ebselen (55) inhibited PL^{pro}, with IC₅₀ values of 7.52 and 2.36 μM, respectively. It is noted that the enzymatic inhibition might be a combined effect of targeting both the catalytic C111 and the cysteines in the ZBD. A combination experiment showed that ebselen and disulfiram had synergistic antiviral effects when combined with hydroxychloroquine. This study suggested that clinically safe zinc ejectors could potentially target the conserved ZBD in multiple viral proteins and could potentially be exploited as broad-spectrum antiviral drug candidates. Following studies from the same group further showed that disulfiram (67) and ebselen (55) are zinc-ejectors of the SARS-CoV-2 nsp13 and nsp14 and consequently inhibit nsp13 ATPase and nsp14 exoribonuclease activities.¹⁰¹ The antiviral activity of ebselen (55) and disulfiram (67) against SARS-CoV-2 was synergistic with remdesivir.

As discussed above, ebselen analogs have also been extensively exploited as M^{pro} and PL^{pro} inhibitors by targeting the active-site cysteine.^{102,103} Combined with the zinc-ejecting property, the antiviral activity of ebselen (55) and its derivatives might be due to its polypharmacology in targeting the ZBD, PL^{pro}, M^{pro}, and others.

4. PERSPECTIVES ON TARGETING THE SARS-CoV-2 PL^{pro}

The COVID-19 pandemic is a timely call for the immediate need for antivirals. As the SARS-CoV and MERS-CoV epidemics subsided, the interest in developing coronavirus inhibitors unfortunately waned, and no significant efforts were devoted to optimizing the hits identified from early high-throughput screening campaigns. Nevertheless, the COVID-19 pandemic re-ignited the interest in PL^{pro} drug discovery, and the past 2 years have seen encouraging progress in the field. Although drug repurposing largely failed to identify potent and selective PL^{pro} inhibitors, rational design based on the X-ray crystal structures led to major breakthroughs, including the design of 2-phenylthiophene PL^{pro} inhibitors with favorable PK properties and the first-in-class covalent PL^{pro} inhibitors since the pandemic. In light of this encouraging progress, we hereby share our opinions on the further development of SARS-CoV-2 PL^{pro} inhibitors, and we hope to clarify some of the confusions in the field based on our experience.

First, there is a need to broaden the antiviral spectrum of PL^{pro} inhibitors to target MERS-CoV. The BL2 loop located at the drug-binding site is poorly conserved among SARS-CoV and MERS-CoV,¹⁰⁴ explaining the lack of activity of the GRL0617

(4) series of compounds against MERS-CoV PL^{pro}. No potent and specific MERS-CoV PL^{pro} inhibitors have been reported until now. In the search for PL^{pro} inhibitors with a broader spectrum of antiviral activity, it is worthwhile to include MERS-CoV PL^{pro} in the secondary assays. It might be possible to identify allosteric inhibitors with dual inhibitions against both SARS-CoV-2 PL^{pro} and MERS-CoV PL^{pro}. Alternatively, PL^{pro} inhibitors can be developed specifically for SARS-CoV-2 and SARS-CoV, and MERS-CoV PL^{pro} inhibitors can be pursued separately.

Second, structurally disparate PL^{pro} inhibitors are needed to advance PL^{pro} inhibitors to the clinic. Compared to PL^{pro}, M^{pro} is a more amenable drug target, and structurally disparate inhibitors have been identified from HTS as potent M^{pro} inhibitors. In contrast, several recent HTS failed to identify additional potent and selective SARS-CoV-2 PL^{pro} inhibitors other than GRL0617 analogues.^{67,85} GRL0617 (4) contains the naphthalene ring, which is a known metabolic labile group and a possible toxicophore.¹⁰⁵ Therefore, it might present a challenge in PK optimization. To increase the chances of success, additional structurally disparate PL^{pro} inhibitors are needed as backups. The recent elegantly designed 2-phenylthiophene and the covalent PL^{pro} inhibitors are prominent examples in this direction.^{67,87}

Third, target selectivity needs to be addressed at an early stage of development. Although there is a lack of sequence or structural similarity between PL^{pro} and human DUBs, both PL^{pro} and human DUBs bind ubiquitin at the extended C-terminus with the consensus sequence Leu-X-Gly-Gly, raising the potential concern about off-target effects of PL^{pro} inhibitors against human DUBs.¹⁰⁶ Consequently, it is important to conduct counter screening of PL^{pro} inhibitors against a panel of related human DUBs to avoid potential toxicity. Along this line, counter screening should also be conducted with other cysteine proteases like the M^{pro}, cathepsin L, calpains, etc. to rule out promiscuous inhibitors that non-specifically inhibit unrelated proteases.

Fourth, be aware of promiscuous inhibitors and compounds with polypharmacology. Promiscuous compounds are defined as compounds that lack a defined mechanism of action or compounds that showed inconsistent results in different assays. PL^{pro} is a cysteine protease that is prone to non-specific inhibition by redox cycling compounds (quinone, arylsulfonamide, tolyl-hydrazide, etc.),^{107,108} alkylating reagents, and other pan-assay interference compounds (PAINS).^{109–111} In addition, compounds such as acriflavine and YM155 are cationic amphiphilic drugs (CADs), which could cause phospholipidosis and disturb endosome/lysosome functions. This effect may explain the improved antiviral potency over biochemical potency. In this regard, the antiviral activity of acriflavine and YM155 might be a combined effect of PL^{pro} inhibition and endosome/lysosome disruption. Furthermore, it is better to perform the antiviral assays in different cell lines, especially in physiologically relevant cell lines such as Calu3 or normal human airway epithelial cells. This eliminates the cell-type-dependent antiviral activity of certain compounds.

Fifth, for translational drug discovery, we need to differentiate chemical probes from drug candidates. Compounds such as ebselen and disulfiram, having non-specific inhibition against PL^{pro} and M^{pro} as well as other unrelated cysteine proteases, should not be classified as PL^{pro} inhibitors. Nevertheless, this does not indicate that these promiscuous compounds should not be further pursued as SARS-CoV-2 antivirals. Instead, they

should be defined as chemical probes for mechanistic studies. The aforementioned cell-based protease assays, such as the FlipGFP and Protease-Glo luciferase assays, are valuable tools to help rule out promiscuous compounds like ebselen and disulfiram and delineate the cellular target engagement of the specific PL^{pro} inhibitors.

In summary, despite the encouraging progress in the past 2 years, there is still a long journey to advance PL^{pro} inhibitors to the clinic. No rationally designed drug-like PL^{pro} inhibitors have been shown to have *in vivo* antiviral efficacy against SARS-CoV-2 infection in animal models yet. In addition to the RdRp and M^{pro} inhibitors, PL^{pro} inhibitors are expected to enrich our armamentarium in fighting the current COVID-19 pandemic and future unforeseeable coronavirus outbreaks. Combination experiments need to be planned to characterize the combination therapy potential of PL^{pro} inhibitors with RdRp or M^{pro} inhibitors. Furthermore, the knowledge accumulated in developing SARS-CoV-2 PL^{pro} inhibitors can be similarly applied to MERS-CoV PL^{pro}.

■ AUTHOR INFORMATION

Corresponding Author

Jun Wang – Department of Medicinal Chemistry, Ernest Mario School of Pharmacy, Rutgers, the State University of New Jersey, Piscataway, New Jersey 08854, United States;
orcid.org/0000-0002-4845-4621; Phone: 848-445-6488;
Email: junwang@pharmacy.rutgers.edu

Authors

Haozhou Tan – Department of Medicinal Chemistry, Ernest Mario School of Pharmacy, Rutgers, the State University of New Jersey, Piscataway, New Jersey 08854, United States
Yanmei Hu – Department of Medicinal Chemistry, Ernest Mario School of Pharmacy, Rutgers, the State University of New Jersey, Piscataway, New Jersey 08854, United States
Prakash Jadhav – Department of Medicinal Chemistry, Ernest Mario School of Pharmacy, Rutgers, the State University of New Jersey, Piscataway, New Jersey 08854, United States
Bin Tan – Department of Medicinal Chemistry, Ernest Mario School of Pharmacy, Rutgers, the State University of New Jersey, Piscataway, New Jersey 08854, United States

Complete contact information is available at:

<https://pubs.acs.org/10.1021/acs.jmedchem.2c00303>

Notes

The authors declare the following competing financial interest(s): Dr. Jun Wang is an inventor of a patent filed for the SARS-CoV-2 PL^{pro} inhibitors.

Biographies

Haozhou Tan earned his B.S. degree from the Hunan Agricultural University (2016, Changsha, China) and master's degree from Northeastern University (2018, Boston, Massachusetts). In 2020, he joined Dr. Jun Wang's lab as a graduate student at the College of Pharmacy, University of Arizona. In 2022, he relocated to the Ernest Mario School of Pharmacy, Rutgers University, with his PI Dr. Wang. His current study focuses on antiviral drug research for influenza and coronavirus.

Yanmei Hu earned her Ph.D. degree from the University of Arizona in August 2021. She continued the postdoctoral training with Dr. Jun Wang and relocated with the Wang laboratory to the Ernest Mario School of Pharmacy, Rutgers University, in 2022. Her current research interests include antiviral drug discovery, assay development, drug

resistance mechanism study, and combination therapy targeting enteroviruses and coronaviruses.

Prakash Jadhav obtained his M.Sc. in chemistry from Pune University, India, in 2011, and then joined Dr. D. S. Reddy's research group as a research assistant in the CSIR-National Chemical Laboratory, Pune. He received his Ph.D. in 2019 from the National Tsing-Hua University, Taiwan, under the supervision of Dr. R. S. Liu and continued his postdoctoral studies with the same research group. After completion of his postdoctoral work in the group of Dr. S. C. Hung at the Genomics Research Center, Academia Sinica, Taiwan, he joined Dr. Jun Wang's group as a postdoctoral researcher in January 2022. His research interests include the design of SARS-CoV-2 PL^{pro} inhibitors.

Bin Tan received his bachelor's and master's degrees from the China Pharmaceutical University in 2018 and 2020, respectively. After graduation, he worked for one year as a research assistant in Dr. Jing Xu's group at the Southern University of Science and Technology. He is now a first-year Ph.D. student in Dr. Jun Wang's lab at Rutgers University, and his research interests include drug discovery targeting SARS-CoV-2 M^{pro} and PL^{pro}.

Jun Wang earned his Ph.D. degree from the University of Pennsylvania in 2010. He continued the postdoctoral training with Dr. William F. DeGrado at the University of California, San Francisco. In 2014, he started an independent career as an assistant professor at the College of Pharmacy, University of Arizona. He was promoted to associate professor in 2020. In 2022, he relocated his lab to the Ernest Mario School of Pharmacy at Rutgers University. His current research interests include antiviral drug discovery, assay development, drug resistance, and combination therapy. Dr. Wang serves as an associate editor and editorial board member for multiple journals including *Journal of Medical Virology*, *Acta Pharmaceutica Sinica B*, *Medicinal Research Reviews*, and *European Journal of Pharmaceutical Sciences*.

ACKNOWLEDGMENTS

This work was supported by the National Institute of Allergy and Infectious Diseases of Health (NIH-NIAID) grants AI147325, AI157046, and AI158775.

ABBREVIATIONS USED

ACE2, angiotensin converting enzyme 2; BRET, bioluminescence resonance energy transfer; BSL-3, biological safety level 3; COVID-19, coronavirus disease 2019; DTT, dithiothreitol; DUBs, deubiquitinases; ESI, electrospray ionization; FITC, fluorescein 5-isothiocyanate; FRET, fluorescence resonance energy transfer; HBA, 4-hydroxybenzaldehyde; HE9, methyl 3, 4-dihydroxybenzoate; i.m., intramuscular; i.p., intraperitoneal; ITC, isothermal titration calorimetry; i.v., intravenous; MALDI-TOF, matrix-assisted laser desorption/ionization time-of-flight; M^{pro}, main protease; NSP, non-structural protein; PAINS, pan-assay interference compounds; PDC, peptide–drug conjugate; PK, pharmacokinetic; PL^{pro}, papain-like protease; RdRp, RNA-dependent RNA polymerase; SPR, surface plasma resonance; 6-TG, 6-thioguanine; VOC, variants of concern; VOI, variants of interests; YRL, 4-(2-hydroxyethyl)phenol; ZBD, zinc-binding domain

REFERENCES

- (1) Liu, D. X.; Liang, J. Q.; Fung, T. S. Human coronavirus-229E, -OC43, -NL63, and -HKU1 (Coronaviridae). *Encyclopedia of Virology* **2021**, 428–440.
- (2) Chen, B.; Tian, E. K.; He, B.; Tian, L.; Han, R.; Wang, S.; Xiang, Q.; Zhang, S.; El Arnaout, T.; Cheng, W. Overview of lethal human coronaviruses. *Signal. Transduct. Target Ther.* **2020**, *5*, 89.
- (3) Cui, J.; Li, F.; Shi, Z. L. Origin and evolution of pathogenic coronaviruses. *Nat. Rev. Microbiol.* **2019**, *17*, 181–192.
- (4) Pyrc, K.; Berkhout, B.; van der Hoek, L. The novel human coronaviruses NL63 and HKU1. *J. Virol.* **2007**, *81*, 3051–3057.
- (5) Gaunt, E. R.; Hardie, A.; Claas, E. C.; Simmonds, P.; Templeton, K. E. Epidemiology and clinical presentations of the four human coronaviruses 229E, HKU1, NL63, and OC43 detected over 3 years using a novel multiplex real-time PCR method. *J. Clin. Microbiol.* **2010**, *48*, 2940–2947.
- (6) Stadler, K.; Massignani, V.; Eickmann, M.; Becker, S.; Abrignani, S.; Klenk, H. D.; Rappuoli, R. SARS—beginning to understand a new virus. *Nat. Rev. Microbiol.* **2003**, *1*, 209–18.
- (7) Chafekar, A.; Fielding, B. C. MERS-CoV: Understanding the latest human coronavirus threat. *Viruses* **2018**, *10*, 93.
- (8) Zhu, N.; Zhang, D.; Wang, W.; Li, X.; Yang, B.; Song, J.; Zhao, X.; Huang, B.; Shi, W.; Lu, R.; Niu, P.; Zhan, F.; Ma, X.; Wang, D.; Xu, W.; Wu, G.; Gao, G. F.; Tan, W. China Novel Coronavirus Investigating and Research Team. A novel coronavirus from patients with pneumonia in China, 2019. *N. Engl. J. Med.* **2020**, *382*, 727–733.
- (9) Wu, F.; Zhao, S.; Yu, B.; Chen, Y. M.; Wang, W.; Song, Z. G.; Hu, Y.; Tao, Z. W.; Tian, J. H.; Pei, Y. Y.; Yuan, M. L.; Zhang, Y. L.; Dai, F. H.; Liu, Y.; Wang, Q. M.; Zheng, J. J.; Xu, L.; Holmes, E. C.; Zhang, Y. Z. A new coronavirus associated with human respiratory disease in China. *Nature* **2020**, *579*, 265–269.
- (10) Hu, B.; Guo, H.; Zhou, P.; Shi, Z. L. Characteristics of SARS-CoV-2 and COVID-19. *Nat. Rev. Microbiol.* **2021**, *19*, 141–154.
- (11) World Health Organization. *WHO Coronavirus (COVID-19) Dashboard*. <https://covid19.who.int/> (accessed May 3, 2022).
- (12) Boras, B.; Jones, R. M.; Anson, B. J.; Arenson, D.; Aschenbrenner, L.; Bakowski, M. A.; Beutler, N.; Binder, J.; Chen, E.; Eng, H.; Hammond, H.; Hammond, J.; Haupt, R. E.; Hoffman, R.; Kadar, E. P.; Kania, R.; Kimoto, E.; Kirkpatrick, M. G.; Lanyon, L.; Lendy, E. K.; Lillis, J. R.; Logue, J.; Luthra, S. A.; Ma, C.; Mason, S. W.; McGrath, M. E.; Noell, S.; Obach, R. S.; O'Brien, M. N.; O'Connor, R.; Ogilvie, K.; Owen, D.; Pettersson, M.; Reese, M. R.; Rogers, T. F.; Rosales, R.; Rossulek, M. I.; Sathish, J. G.; Shirai, N.; Stepan, C.; Ticehurst, M.; Updyke, L. W.; Weston, S.; Zhu, Y.; White, K. M.; Garcia-Sastre, A.; Wang, J.; Chatterjee, A. K.; Mesecar, A. D.; Frieman, M. B.; Anderson, A. S.; Allerton, C. Preclinical characterization of an intravenous coronavirus 3CL protease inhibitor for the potential treatment of COVID-19. *Nat. Commun.* **2021**, *12*, 6055.
- (13) Owen, D. R.; Allerton, C. M. N.; Anderson, A. S.; Aschenbrenner, L.; Avery, M.; Berritt, S.; Boras, B.; Cardin, R. D.; Carlo, A.; Coffman, K. J.; Dantonio, A.; Di, L.; Eng, H.; Ferre, R.; Gajiwala, K. S.; Gibson, S. A.; Greasley, S. E.; Hurst, B. L.; Kadar, E. P.; Kalgutkar, A. S.; Lee, J. C.; Lee, J.; Liu, W.; Mason, S. W.; Noell, S.; Novak, J. J.; Obach, R. S.; Ogilvie, K.; Patel, N. C.; Pettersson, M.; Rai, D. K.; Reese, M. R.; Sammons, M. F.; Sathish, J. G.; Singh, R. S. P.; Stepan, C. M.; Stewart, A. E.; Tuttle, J. B.; Updyke, L.; Verhoest, P. R.; Wei, L.; Wang, Q.; Zhu, Y. An oral SARS-CoV-2 M^{pro} inhibitor clinical candidate for the treatment of COVID-19. *Science* **2021**, *374*, 1586–1593.
- (14) Li, Y.; Tenchov, R.; Smoot, J.; Liu, C.; Watkins, S.; Zhou, Q. A comprehensive review of the global efforts on COVID-19 vaccine development. *ACS Cent. Sci.* **2021**, *7*, 512–533.
- (15) Tregoning, J. S.; Flight, K. E.; Higham, S. L.; Wang, Z.; Pierce, B. F. Progress of the COVID-19 vaccine effort: viruses, vaccines and variants versus efficacy, effectiveness and escape. *Nat. Rev. Immunol.* **2021**, *21*, 626–636.
- (16) Ghosh, A. K.; Brindisi, M.; Shahabi, D.; Chapman, M. E.; Mesecar, A. D. Drug development and medicinal chemistry efforts toward SARS-coronavirus and Covid-19 therapeutics. *ChemMedChem* **2020**, *15*, 907–932.
- (17) Morse, J. S.; Lalonde, T.; Xu, S.; Liu, W. R. Learning from the past: possible urgent prevention and treatment options for severe acute respiratory infections caused by 2019-nCoV. *ChemBiochem* **2020**, *21*, 730–738.
- (18) Beigel, J. H.; Tomashek, K. M.; Dodd, L. E.; Mehta, A. K.; Zingman, B. S.; Kalil, A. C.; Hohmann, E.; Chu, H. Y.; Luetkemeyer, A.; Kline, S.; Lopez de Castilla, D.; Finberg, R. W.; Dierberg, K.; Tapson,

- V.; Hsieh, L.; Patterson, T. F.; Paredes, R.; Sweeney, D. A.; Short, W. R.; Touloumi, G.; Lye, D. C.; Ohmagari, N.; Oh, M.-d.; Ruiz-Palacios, G. M.; Benfield, T.; Fätkenheuer, G.; Kortepeter, M. G.; Atmar, R. L.; Creech, C. B.; Lundgren, J.; Babiker, A. G.; Pett, S.; Neaton, J. D.; Burgess, T. H.; Bonnett, T.; Green, M.; Makowski, M.; Osinusi, A.; Nayak, S.; Lane, H. C. Remdesivir for the treatment of Covid-19 — final report. *N. Engl. J. Med.* **2020**, *383*, 1813–1826.
- (19) Yin, W.; Mao, C.; Luan, X.; Shen, D. D.; Shen, Q.; Su, H.; Wang, X.; Zhou, F.; Zhao, W.; Gao, M.; Chang, S.; Xie, Y. C.; Tian, G.; Jiang, H. W.; Tao, S. C.; Shen, J.; Jiang, Y.; Jiang, H.; Xu, Y.; Zhang, S.; Zhang, Y.; Xu, H. E. Structural basis for inhibition of the RNA-dependent RNA polymerase from SARS-CoV-2 by remdesivir. *Science* **2020**, *368*, 1499–1504.
- (20) Cox, R. M.; Wolf, J. D.; Plemper, R. K. Therapeutically administered ribonucleoside analogue MK-4482/EIDD-2801 blocks SARS-CoV-2 transmission in ferrets. *Nat. Microbiol.* **2021**, *6*, 11–18.
- (21) Jayk Bernal, A.; Gomes da Silva, M. M.; Musungaie, D. B.; Kovalchuk, E.; Gonzalez, A.; Delos Reyes, V.; Martin-Quiros, A.; Caraco, Y.; Williams-Diaz, A.; Brown, M. L.; Du, J.; Pedley, A.; Assaid, C.; Strizki, J.; Grobler, J. A.; Shamsuddin, H. H.; Tipping, R.; Wan, H.; Paschke, A.; Butterton, J. R.; Johnson, M. G.; De Anda, C. MOVE-OUT Study Group. Molnupiravir for oral treatment of Covid-19 in nonhospitalized patients. *N. Engl. J. Med.* **2022**, *386*, 509–520.
- (22) Kabinger, F.; Stiller, C.; Schmitzova, J.; Dienemann, C.; Kocic, G.; Hillen, H. S.; Hobartner, C.; Cramer, P. Mechanism of molnupiravir-induced SARS-CoV-2 mutagenesis. *Nat. Struct. Mol. Biol.* **2021**, *28*, 740–746.
- (23) Painter, W. P.; Holman, W.; Bush, J. A.; Almazedi, F.; Malik, H.; Eraut, N.; Morin, M. J.; Szewczyk, L. J.; Painter, G. R. Human safety, tolerability, and pharmacokinetics of molnupiravir, a novel broad-spectrum oral antiviral agent with activity against SARS-CoV-2. *Antimicrob. Agents Chemother.* **2021**, *65*, e02428-20.
- (24) Liu, C.; Zhou, C.; Li, Y.; Garner, L. V.; Watkins, S. P.; Carter, L. J.; Smoot, J.; Gregg, A. C.; Daniels, A. D.; Jervey, S.; Albaiu, D. Research and development on therapeutic agents and vaccines for COVID-19 and related human coronavirus diseases. *ACS Cent. Sci.* **2020**, *6*, 315–331.
- (25) Harvey, W. T.; Carabelli, A. M.; Jackson, B.; Gupta, R. K.; Thomson, E. C.; Harrison, E. M.; Ludden, C.; Reeve, R.; Rambaut, A.; Peacock, S. J.; Robertson, D. L.; COVID-19 Genomics UK (COG-UK) Consortium. SARS-CoV-2 variants, spike mutations and immune escape. *Nat. Rev. Microbiol.* **2021**, *19*, 409–424.
- (26) Supasa, P.; Zhou, D.; Dejnirattisai, W.; Liu, C.; Mentzer, A. J.; Ginn, H. M.; Zhao, Y.; Duyvesteyn, H. M. E.; Nutalai, R.; Tuekprakhon, A.; Wang, B.; Paesen, G. C.; Slon-Campos, J.; Lopez-Camacho, C.; Hallis, B.; Coombes, N.; Bewley, K. R.; Charlton, S.; Walter, T. S.; Barnes, E.; Dunachie, S. J.; Skelly, D.; Lumley, S. F.; Baker, N.; Shaik, I.; Humphries, H. E.; Godwin, K.; Gent, N.; Sienkiewicz, A.; Dold, C.; Levin, R.; Dong, T.; Pollard, A. J.; Knight, J. C.; Klenerman, P.; Crook, D.; Lambe, T.; Clutterbuck, E.; Bibi, S.; Flaxman, A.; Bittaye, M.; Belij-Rammerstorfer, S.; Gilbert, S.; Hall, D. R.; Williams, M. A.; Paterson, N. G.; James, W.; Carroll, M. W.; Fry, E. E.; Mongkolsapaya, J.; Ren, J.; Stuart, D. I.; Sreaton, G. R. Reduced neutralization of SARS-CoV-2 B.1.1.7 variant by convalescent and vaccine sera. *Cell* **2021**, *184*, 2201–2211.e7.
- (27) VanBlargan, L. A.; Errico, J. M.; Halfmann, P. J.; Zost, S. J.; Crowe, J. E., Jr; Purcell, L. A.; Kawaoka, Y.; Corti, D.; Fremont, D. H.; Diamond, M. S. An infectious SARS-CoV-2 B.1.1.529 Omicron virus escapes neutralization by therapeutic monoclonal antibodies. *Nat. Med.* **2022**, *28*, 490–495.
- (28) Szemiel, A. M.; Merits, A.; Orton, R. J.; MacLean, O. A.; Pinto, R. M.; Wickenhagen, A.; Lieber, G.; Turnbull, M. L.; Wang, S.; Furnon, W.; Suarez, N. M.; Mair, D.; da Silva Filipe, A.; Willett, B. J.; Wilson, S. J.; Patel, A. H.; Thomson, E. C.; Palmarini, M.; Kohl, A.; Stewart, M. E. In vitro selection of Remdesivir resistance suggests evolutionary predictability of SARS-CoV-2. *PLoS Pathog.* **2021**, *17*, No. e1009929.
- (29) Stevens, L. J.; Pruijssers, A. J.; Lee, H. W.; Gordon, C. J.; Tchesnokov, E. P.; Gribble, J.; George, A. S.; Hughes, T. M.; Lu, X.; Li, J.; Perry, J. K.; Porter, D. P.; Cihlar, T.; Sheahan, T. P.; Baric, R. S.; Götte, M.; Denison, M. R. Mutations in the SARS-CoV-2 RNA dependent RNA polymerase confer resistance to remdesivir by distinct mechanisms. *Sci. Transl. Med.* **2022**, eabo0718.
- (30) Focosi, D.; Maggi, F.; McConnell, S.; Casadevall, A. Very low levels of remdesivir resistance in SARS-CoV-2 genomes after 18 months of massive usage during the COVID19 pandemic: A GISAID exploratory analysis. *Antiviral Res.* **2022**, *198*, 105247.
- (31) Wang, Y.; Zhang, D.; Du, G.; Du, R.; Zhao, J.; Jin, Y.; Fu, S.; Gao, L.; Cheng, Z.; Lu, Q.; Hu, Y.; Luo, G.; Wang, K.; Lu, Y.; Li, H.; Wang, S.; Ruan, S.; Yang, C.; Mei, C.; Wang, Y.; Ding, D.; Wu, F.; Tang, X.; Ye, X.; Ye, Y.; Liu, B.; Yang, J.; Yin, W.; Wang, A.; Fan, G.; Zhou, F.; Liu, Z.; Gu, X.; Xu, J.; Shang, L.; Zhang, Y.; Cao, L.; Guo, T.; Wan, Y.; Qin, H.; Jiang, Y.; Jaki, T.; Hayden, F. G.; Horby, P. W.; Cao, B.; Wang, C. Remdesivir in adults with severe COVID-19: a randomised, double-blind, placebo-controlled, multicentre trial. *Lancet* **2020**, *395*, 1569–1578.
- (32) Spinner, C. D.; Gottlieb, R. L.; Criner, G. J.; Arribas Lopez, J. R.; Cattelan, A. M.; Soriano Viladomiu, A.; Ogbuagu, O.; Malhotra, P.; Mullane, K. M.; Castagna, A.; Chai, L. Y. A.; Roestenberg, M.; Tsang, O. T. Y.; Bernasconi, E.; Le Turnier, P.; Chang, S. C.; SenGupta, D.; Hyland, R. H.; Osinusi, A. O.; Cao, H.; Blair, C.; Wu, F.; Gaggar, A.; Brainard, D. M.; McPhail, M. J.; Bhagani, S.; Ahn, M. Y.; Sanyal, A. J.; Huhn, G.; Marty, F. M. GS-US-540–5774 Investigators. Effect of remdesivir vs standard care on clinical status at 11 days in patients with moderate COVID-19: a randomized clinical trial. *JAMA* **2020**, *324*, 1048–1057.
- (33) Swanstrom, R.; Schinazi, R. F. Lethal mutagenesis as an antiviral strategy. *Science* **2022**, *375*, 497–498.
- (34) Zhou, S.; Hill, C. S.; Sarkar, S.; Tse, L. V.; Woodburn, B. M. D.; Schinazi, R. F.; Sheahan, T. P.; Baric, R. S.; Heise, M. T.; Swanstrom, R. Beta-d-N4-hydroxycytidine inhibits SARS-CoV-2 through lethal mutagenesis but is also mutagenic to mammalian cells. *J. Infect. Dis.* **2021**, *224*, 415–419.
- (35) U.S. FDA. *Fact sheet for healthcare providers: Emergency use authorization for molnupiravir*, December 2021. www.fda.gov/media/155054/download (accessed May 5, 2022).
- (36) Sacco, M. D.; Hu, Y. M.; Gongora, M. V.; Meilleur, F.; Kemp, M. T.; Zhang, X. J.; Wang, J.; Chen, Y. The P132H mutation in the main protease of Omicron SARS-CoV-2 decreases thermal stability without compromising catalysis or small-molecule drug inhibition. *Cell. Res.* **2022**, *32*, 498–500.
- (37) Greasley, S. E.; Noell, S.; Plotnikova, O.; Ferre, R. A.; Liu, W.; Bolanos, B.; Fennell, K.; Nicki, J.; Craig, T.; Zhu, Y.; Stewart, A. E.; Stepan, C. M. Structural basis for Nirmatrelvir in vitro efficacy against the Omicron variant of SARS-CoV-2. *J. Biol. Chem.* **2022**, *101972*.
- (38) Ullrich, S.; Ekanayake, K. B.; Otting, G.; Nitsche, C. Main protease mutants of SARS-CoV-2 variants remain susceptible to nirmatrelvir (PF-07321332). *Bioorg. Med. Chem. Lett.* **2022**, *62*, 128629.
- (39) U.S. FDA. *Fact sheet for healthcare providers: Emergency use authorization for Paxlovid*, December 2021. <https://www.fda.gov/media/155050/download> (accessed May 5, 2022).
- (40) Matthew, A. N.; Leidner, F.; Lockbaum, G. J.; Henes, M.; Zephyr, J.; Hou, S.; Rao, D. N.; Timm, J.; Rusere, L. N.; Ragland, D. A.; Paulsen, J. L.; Prachanronarong, K.; Soumana, D. I.; Nalivaika, E. A.; Kurt Yilmaz, N.; Ali, A.; Schiffer, C. A. Drug design strategies to avoid resistance in direct-acting antivirals and beyond. *Chem. Rev.* **2021**, *121*, 3238–3270.
- (41) Heskin, J.; Pallett, S. J. C.; Mughal, N.; Davies, G. W.; Moore, L. S. P.; Rayment, M.; Jones, R. Caution required with use of ritonavir-boosted PF-07321332 in COVID-19 management. *Lancet* **2022**, *399*, 21–22.
- (42) Mielech, A. M.; Kilianski, A.; Baez-Santos, Y. M.; Mesecar, A. D.; Baker, S. C. MERS-CoV papain-like protease has deISGylating and deubiquitinating activities. *Virology* **2014**, *450–451*, 64–70.
- (43) Sulea, T.; Lindner, H. A.; Purisima, E. O.; Menard, R. Deubiquitination, a new function of the severe acute respiratory syndrome coronavirus papain-like protease? *J. Virol.* **2005**, *79*, 4550–4551.

- (44) Bekes, M.; van der Heden van Noort, G. J.; Ekkebus, R.; Ovaa, H.; Huang, T. T.; Lima, C. D. Recognition of lys48-linked di-ubiquitin and deubiquitinating activities of the SARS coronavirus papain-like protease. *Mol. Cell* **2016**, *62*, 572–585.
- (45) Freitas, B. T.; Durie, I. A.; Murray, J.; Longo, J. E.; Miller, H. C.; Crich, D.; Hogan, R. J.; Tripp, R. A.; Pegan, S. D. Characterization and noncovalent inhibition of the deubiquitinase and deISGylase activity of SARS-CoV-2 papain-like protease. *ACS Infect. Dis.* **2020**, *6*, 2099–2109.
- (46) Shin, D.; Mukherjee, R.; Grewe, D.; Bojkova, D.; Baek, K.; Bhattacharya, A.; Schulz, L.; Widera, M.; Mehdipour, A. R.; Tascher, G.; Geurink, P. P.; Wilhelm, A.; van der Heden van Noort, G. J.; Ovaa, H.; Müller, S.; Knobloch, K.-P.; Rajalingam, K.; Schulman, B. A.; Cinatl, J.; Hummer, G.; Ciesek, S.; Dikic, I. Papain-like protease regulates SARS-CoV-2 viral spread and innate immunity. *Nature* **2020**, *587*, 657–662.
- (47) Munnur, D.; Teo, Q.; Eggermont, D.; Lee, H. H. Y.; Thery, F.; Ho, J.; van Leur, S. W.; Ng, W. W. S.; Siu, L. Y. L.; Beling, A.; Ploegh, H.; Pinto-Fernandez, A.; Damianou, A.; Kessler, B.; Impens, F.; Mok, C. K. P.; Sanyal, S. Altered ISGylation drives aberrant macrophage-dependent immune responses during SARS-CoV-2 infection. *Nat. Immunol.* **2021**, *22*, 1416–1427.
- (48) Cao, X. ISG15 secretion exacerbates inflammation in SARS-CoV-2 infection. *Nat. Immunol.* **2021**, *22*, 1360–1362.
- (49) Lei, J.; Kusov, Y.; Hilgenfeld, R. Nsp3 of coronaviruses: structures and functions of a large multi-domain protein. *Antiviral Res.* **2018**, *149*, 58–74.
- (50) Woo, P. C.; Huang, Y.; Lau, S. K.; Yuen, K. Y. Coronavirus genomics and bioinformatics analysis. *Viruses* **2010**, *2*, 1804–1820.
- (51) Chen, Z.; Wang, Y.; Ratia, K.; Mesecar, A. D.; Wilkinson, K. D.; Baker, S. C. Proteolytic processing and deubiquitinating activity of papain-like proteases of human coronavirus NL63. *J. Virol.* **2007**, *81*, 6007–6018.
- (52) Osipiuk, J.; Azizi, S. A.; Dvorkin, S.; Endres, M.; Jedrzejczak, R.; Jones, K. A.; Kang, S.; Kathayat, R. S.; Kim, Y.; Lisnyak, V. G.; Maki, S. L.; Nicolaescu, V.; Taylor, C. A.; Tesar, C.; Zhang, Y. A.; Zhou, Z.; Randall, G.; Michalska, K.; Snyder, S. A.; Dickinson, B. C.; Joachimiak, A. Structure of papain-like protease from SARS-CoV-2 and its complexes with non-covalent inhibitors. *Nat. Commun.* **2021**, *12*, 743.
- (53) Klemm, T.; Ebert, G.; Calleja, D. J.; Allison, C. C.; Richardson, L. W.; Bernardini, J. P.; Lu, B. G.; Kuchel, N. W.; Grohmann, C.; Shibata, Y.; Gan, Z. Y.; Cooney, J. P.; Doerflinger, M.; Au, A. E.; Blackmore, T. R.; Heden van Noort, G. J.; Geurink, P. P.; Ovaa, H.; Newman, J.; Riboldi-Tunnichiffe, A.; Czabotar, P. E.; Mitchell, J. P.; Feltham, R.; Lechtenberg, B. C.; Lowes, K. N.; Dewson, G.; Pellegrini, M.; Lessene, G.; Komander, D. Mechanism and inhibition of the papain-like protease, PLpro, of SARS-CoV-2. *EMBO J.* **2020**, *39*, No. e106275.
- (54) Ma, C.; Sacco, M. D.; Xia, Z.; Lambrinidis, G.; Townsend, J. A.; Hu, Y.; Meng, X.; Szeto, T.; Ba, M.; Zhang, X.; Gongora, M.; Zhang, F.; Marty, M. T.; Xiang, Y.; Kolocouris, A.; Chen, Y.; Wang, J. Discovery of SARS-CoV-2 papain-like protease inhibitors through a combination of high-throughput screening and a FlipGFP-based reporter assay. *ACS Cent. Sci.* **2021**, *7*, 1245–1260.
- (55) Srinivasan, V.; Brognaro, H.; Prabhu, P. R.; de Souza, E. E.; Günther, S.; Reinke, P. Y. A.; Lane, T. J.; Ginn, H.; Han, H.; Ewert, W.; Sprenger, J.; Koua, F. H. M.; Falke, S.; Werner, N.; Andaleeb, H.; Ullah, N.; Franca, B. A.; Wang, M.; Barra, A. L. C.; Perbandt, M.; Schwinzer, M.; Schmidt, C.; Brings, L.; Lorenzen, K.; Schubert, R.; Guaragna Machado, R. R.; Candido, E. D.; Leal Oliveira, D. B.; Durigon, E. L.; Yefanov, O.; Lieske, J.; Gelisio, L.; Domaracky, M.; Middendorf, P.; Groessler, M.; Trost, F.; Galchenkova, M.; Saouane, S.; Hakanpää, J.; Wolf, M.; Turk, D.; Pearson, A. R.; Chapman, H. N.; Hinrichs, W.; Wrenger, C.; Meents, A.; Betzel, C. SARS-CoV-2 papain-like protease PLpro in complex with natural compounds reveal allosteric sites for antiviral drug design. *bioRxiv* **2021**, DOI: 10.1101/2021.11.17.468943v1.
- (56) Osipiuk, J.; Wydorski, P. M.; Lanham, B. T.; Tesar, C.; Endres, M.; Engle, E.; Jedrzejczak, R.; Mullapudi, V.; Michalska, K.; Fidelis, K.; Fushman, D.; Joachimiak, A.; Joachimiak, L. A. Dual domain recognition determines SARS-CoV-2 PLpro selectivity for human ISG15 and K48-linked di-ubiquitin. *bioRxiv* **2021**, DOI: 10.1101/2021.09.15.460543v2.
- (57) Rut, W.; Lv, Z.; Zmudzinski, M.; Patchett, S.; Nayak, D.; Snipas, S. J.; El Oualid, F.; Huang, T. T.; Bekes, M.; Drag, M.; Olsen, S. K. Activity profiling and crystal structures of inhibitor-bound SARS-CoV-2 papain-like protease: A framework for anti-COVID-19 drug design. *Sci. Adv.* **2020**, *6*, eabd4596.
- (58) Baez-Santos, Y. M.; St John, S. E.; Mesecar, A. D. The SARS-coronavirus papain-like protease: structure, function and inhibition by designed antiviral compounds. *Antiviral Res.* **2015**, *115*, 21–38.
- (59) Capasso, C.; Nocentini, A.; Supuran, C. T. Protease inhibitors targeting the main protease and papain-like protease of coronaviruses. *Expert Opin. Ther. Pat.* **2021**, *31*, 309–324.
- (60) Ghosh, A. K.; Takayama, J.; Aubin, Y.; Ratia, K.; Chaudhuri, R.; Baez, Y.; Sleeman, K.; Coughlin, M.; Nichols, D. B.; Mulhearn, D. C.; Prabhakar, B. S.; Baker, S. C.; Johnson, M. E.; Mesecar, A. D. Structure-based design, synthesis, and biological evaluation of a series of novel and reversible inhibitors for the severe acute respiratory syndrome-coronavirus papain-like protease. *J. Med. Chem.* **2009**, *52*, 5228–5240.
- (61) Ghosh, A. K.; Takayama, J.; Rao, K. V.; Ratia, K.; Chaudhuri, R.; Mulhearn, D. C.; Lee, H.; Nichols, D. B.; Baliji, S.; Baker, S. C.; Johnson, M. E.; Mesecar, A. D. Severe acute respiratory syndrome coronavirus papain-like novel protease inhibitors: design, synthesis, protein-ligand X-ray structure and biological evaluation. *J. Med. Chem.* **2010**, *53*, 4968–4979.
- (62) Ratia, K.; Pegan, S.; Takayama, J.; Sleeman, K.; Coughlin, M.; Baliji, S.; Chaudhuri, R.; Fu, W.; Prabhakar, B. S.; Johnson, M. E.; Baker, S. C.; Ghosh, A. K.; Mesecar, A. D. A noncovalent class of papain-like protease/deubiquitinase inhibitors blocks SARS virus replication. *Proc. Natl. Acad. Sci. U. S. A.* **2008**, *105*, 16119–16124.
- (63) Markossian, S.; Grossman, A.; Brimacombe, K.; Arkin, M.; Auld, D.; Austin, P. C.; Baell, J.; Chung, D. Y. T.; Coussens, P. N.; Dahlin, L. J.; Devanarayan, V.; Foley, L. T.; Glicksman, M.; Hall, D. M.; Hass, V. J.; Hoare, R. J. S.; Inglese, J.; Iversen, W. P.; Kales, C. S.; Lal-Nag, M.; Li, Z.; McGee, J.; McManus, O.; Riss, T.; Saradjian, P.; Sittampalam, S. G.; Tarselli, M.; Trask, J. O.; Wang, Y.; Weidner, R. J.; Wildey, J. M.; Wilson, K.; Xia, M.; Xu, X. *Assay Guidance Manual*; Eli Lilly & Company and the National Center for Advancing Translational Sciences: Bethesda, MD, 2004. <https://www.ncbi.nlm.nih.gov/books/NBK53196/> (accessed May 5, 2022).
- (64) Ma, C.; Tan, H.; Choza, J.; Wang, Y.; Wang, J. Validation and invalidation of SARS-CoV-2 main protease inhibitors using the Flip-GFP and Protease-Glo luciferase assays. *Acta Pharm. Sin. B* **2022**, *12*, 1636–1651.
- (65) Ma, C.; Hu, Y.; Townsend, J. A.; Lagarias, P. I.; Marty, M. T.; Kolocouris, A.; Wang, J. Ebselen, disulfiram, carmofur, PX-12, tideglusib, and shikonin are nonspecific promiscuous SARS-CoV-2 main protease inhibitors. *ACS Pharmacol. Transl. Sci.* **2020**, *3*, 1265–1277.
- (66) Ma, C.; Wang, J. Dipyridamole, chloroquine, montelukast sodium, candesartan, oxytetracycline, and atazanavir are not SARS-CoV-2 main protease inhibitors. *Proc. Natl. Acad. Sci. U. S. A.* **2021**, *118*, No. e2024420118.
- (67) Shen, Z.; Ratia, K.; Cooper, L.; Kong, D.; Lee, H.; Kwon, Y.; Li, Y.; Alqarni, S.; Huang, F.; Dubrovskiy, O.; Rong, L.; Thatcher, G. R. J.; Xiong, R. Design of SARS-CoV-2 PLpro inhibitors for COVID-19 antiviral therapy leveraging binding cooperativity. *J. Med. Chem.* **2022**, *65*, 2940–2955.
- (68) Fu, Z.; Huang, B.; Tang, J.; Liu, S.; Liu, M.; Ye, Y.; Liu, Z.; Xiong, Y.; Zhu, W.; Cao, D.; Li, J.; Niu, X.; Zhou, H.; Zhao, Y. J.; Zhang, G.; Huang, H. The complex structure of GRL0617 and SARS-CoV-2 PLpro reveals a hot spot for antiviral drug discovery. *Nat. Commun.* **2021**, *12*, 488.
- (69) Ma, C.; Wang, J. Validation and invalidation of SARS-CoV-2 papain-like protease inhibitors. *ACS Pharmacol. Transl. Sci.* **2022**, *5*, 102–109.
- (70) Li, X.; Lidsky, P. V.; Xiao, Y.; Wu, C. T.; Garcia-Knight, M.; Yang, J.; Nakayama, T.; Nayak, J. V.; Jackson, P. K.; Andino, R.; Shu, X.

- Ethacridine inhibits SARS-CoV-2 by inactivating viral particles. *PLoS Pathog.* **2021**, *17*, No. e1009898.
- (71) Zhang, Q.; Schepis, A.; Huang, H.; Yang, J.; Ma, W.; Torra, J.; Zhang, S. Q.; Yang, L.; Wu, H.; Nonell, S.; Dong, Z.; Kornberg, T. B.; Coughlin, S. R.; Shu, X. Designing a green fluorogenic protease reporter by flipping a beta strand of GFP for imaging apoptosis in animals. *J. Am. Chem. Soc.* **2019**, *141*, 4526–4530.
- (72) Froggatt, H. M.; Heaton, B. E.; Heaton, N. S. Development of a fluorescence-based, high-throughput SARS-CoV-2 3CL(pro) reporter assay. *J. Virol.* **2020**, *94*, e01265-20.
- (73) Ma, C.; Xia, Z.; Sacco, M. D.; Hu, Y.; Townsend, J. A.; Meng, X.; Choza, J.; Tan, H.; Jang, J.; Gongora, M. V.; Zhang, X.; Zhang, F.; Xiang, Y.; Marty, M. T.; Chen, Y.; Wang, J. Discovery of di- and trihaloacetamides as covalent SARS-CoV-2 main protease inhibitors with high target specificity. *J. Am. Chem. Soc.* **2021**, *143*, 20697–20709.
- (74) Rawson, J. M. O.; Duchon, A. V.; Nikolaitchik, O. A.; Pathak, V. K.; Hu, W. S. Development of a cell-based luciferase complementation assay for identification of SARS-CoV-2 3CL(pro) inhibitors. *Viruses* **2021**, *13*, 173.
- (75) Gerber, P. P.; Duncan, L. M.; Greenwood, E. J.; Marelli, S.; Naamati, A.; Teixeira-Silva, A.; Crozier, T. W.; Gabaev, I.; Zhan, J. R.; Mulrone, T. E.; Horner, E. C.; Doffinger, R.; Willis, A. E.; Thaventhiran, J. E.; Protasio, A. V.; Matheson, N. J. A protease-activatable luminescent biosensor and reporter cell line for authentic SARS-CoV-2 infection. *PLoS Pathog.* **2022**, *18*, No. e1010265.
- (76) Pahmeier, F.; Neufeldt, C. J.; Cerikan, B.; Prasad, V.; Pape, C.; Laketa, V.; Ruggieri, A.; Bartenschlager, R.; Cortese, M. A versatile reporter system to monitor virus-infected cells and its application to dengue virus and SARS-CoV-2. *J. Virol.* **2021**, *95*, e01715-20.
- (77) Cao, W.; Cho, C. D.; Geng, Z. Z.; Shaabani, N.; Ma, X. R.; Vatansever, E. C.; Alugubelli, Y. R.; Ma, Y.; Chaki, S. P.; Ellenburg, W. H.; Yang, K. S.; Qiao, Y.; Allen, R.; Neuman, B. W.; Ji, H.; Xu, S.; Liu, W. R. Evaluation of SARS-CoV-2 main protease inhibitors using a novel cell-based assay. *ACS Cent. Sci.* **2022**, *8*, 192–204.
- (78) Gao, X.; Qin, B.; Chen, P.; Zhu, K.; Hou, P.; Wojdyla, J. A.; Wang, M.; Cui, S. Crystal structure of SARS-CoV-2 papain-like protease. *Acta Pharm. Sin. B* **2021**, *11*, 237–245.
- (79) Shan, H.; Liu, J.; Shen, J.; Dai, J.; Xu, G.; Lu, K.; Han, C.; Wang, Y.; Xu, X.; Tong, Y.; Xiang, H.; Ai, Z.; Zhuang, G.; Hu, J.; Zhang, Z.; Li, Y.; Pan, L.; Tan, L. Development of potent and selective inhibitors targeting the papain-like protease of SARS-CoV-2. *Cell Chem. Biol.* **2021**, *28*, 855–865.e9.
- (80) Zhao, Y.; Du, X.; Duan, Y.; Pan, X.; Sun, Y.; You, T.; Han, L.; Jin, Z.; Shang, W.; Yu, J.; Guo, H.; Liu, Q.; Wu, Y.; Peng, C.; Wang, J.; Zhu, C.; Yang, X.; Yang, K.; Lei, Y.; Guddat, L. W.; Xu, W.; Xiao, G.; Sun, L.; Zhang, L.; Rao, Z.; Yang, H. High-throughput screening identifies established drugs as SARS-CoV-2 PLpro inhibitors. *Protein Cell* **2021**, *12*, 877–888.
- (81) Lim, C. T.; Tan, K. W.; Wu, M.; Ulferts, R.; Armstrong, L. A.; Ozono, E.; Drury, L. S.; Milligan, J. C.; Zeisner, T. U.; Zeng, J.; Weissmann, F.; Canal, B.; Bineva-Todd, G.; Howell, M.; O'Reilly, N.; Beale, R.; Kulathu, Y.; Labib, K.; Diffley, J. F. X. Identifying SARS-CoV-2 antiviral compounds by screening for small molecule inhibitors of Nsp3 papain-like protease. *Biochem. J.* **2021**, *478*, 2517–2531.
- (82) Napolitano, V.; Dabrowska, A.; Schorpp, K.; Mourao, A.; Barreto-Duran, E.; Benedyk, M.; Botwina, P.; Brandner, S.; Bostock, M.; Chykunova, Y.; Czarna, A.; Dubin, G.; Frohlich, T.; Holscher, M.; Jedrysik, M.; Matsuda, A.; Owczarek, K.; Pachota, M.; Plettenburg, O.; Potempa, J.; Rothenaigner, I.; Schlauderer, F.; Slys, K.; Szczepanski, A.; Greve-Isdahl Mohn, K.; Blomberg, B.; Sattler, M.; Hadian, K.; Popowicz, G. M.; Pyrc, K. Acriflavine, a clinically approved drug, inhibits SARS-CoV-2 and other betacoronaviruses. *Cell Chem. Biol.* **2022**, DOI: 10.1016/j.chembiol.2021.11.006.
- (83) Xu, Y.; Chen, K.; Pan, J.; Lei, Y.; Zhang, D.; Fang, L.; Tang, J.; Chen, X.; Ma, Y.; Zheng, Y.; Zhang, B.; Zhou, Y.; Zhan, J.; Xu, W. Repurposing clinically approved drugs for COVID-19 treatment targeting SARS-CoV-2 papain-like protease. *Int. J. Biol. Macromol.* **2021**, *188*, 137–146.
- (84) Santos, L. H.; Kronenberger, T.; Almeida, R. G.; Silva, E. B.; Rocha, R. E. O.; Oliveira, J. C.; Barreto, L. V.; Skinner, D.; Fajtova, P.; Giardini, M. A.; Woodworth, B.; Bardine, C.; Lourenco, A. L.; Craik, C. S.; Poso, A.; Podust, L. M.; McKerrow, J. H.; Siqueira-Neto, J. L.; O'Donoghue, A. J.; da Silva Junior, E. N.; Ferreira, R. S. Structure-based identification of naphthoquinones and derivatives as novel inhibitors of main protease Mpro and papain-like protease PLpro of SARS-CoV-2. *bioRxiv* **2022**, DOI: 10.1101/2022.01.05.475095v1.
- (85) Cho, C. C.; Li, S. G.; Lalonde, T. J.; Yang, K. S.; Yu, G.; Qiao, Y.; Xu, S.; Ray Liu, W. Drug repurposing for the SARS-CoV-2 papain-like protease. *ChemMedChem* **2022**, *17*, No. e202100455.
- (86) Lewis, D. S. M.; Ho, J.; Wills, S.; Kawall, A.; Sharma, A.; Chavada, K.; Ebert, M.; Evoli, S.; Singh, A.; Rayalam, S.; Mody, V.; Taval, S. Aoin isoforms (A and B) selectively inhibits proteolytic and deubiquitinating activity of papain like protease (PLpro) of SARS-CoV-2 in vitro. *Sci. Rep.* **2022**, *12*, 2145.
- (87) Sanders, B.; Pohkrel, S.; Labbe, A.; Mathews, I.; Cooper, C.; Davidson, R.; Phillips, G.; Weiss, K.; Zhang, Q.; O'Neill, H.; Kaur, M.; Ferrins, L.; Schmidt, J.; Reichard, W.; Surendranathan, S.; Kumaran, D.; Andi, B.; Babnigg, G.; Moriarty, N.; Adams, P.; Joachimiak, A.; Jonsson, C.; Wakatsuki, S.; Galanie, S.; Head, M.; Parks, J. Potent and selective covalent inhibitors of the papain-like protease from SARS-CoV-2. *Res. Sq.* **2021**, DOI: 10.21203/rs.3.rs-906621/v1.
- (88) Liu, N.; Zhang, Y.; Lei, Y.; Wang, R.; Zhan, M.; Liu, J.; An, Y.; Zhou, Y.; Zhan, J.; Yin, F.; Li, Z. Design and evaluation of a novel peptide–drug conjugate covalently targeting SARS-CoV-2 papain-like protease. *J. Med. Chem.* **2022**, *65*, 876–884.
- (89) Di Sarno, V.; Lauro, G.; Musella, S.; Ciaglia, T.; Vestuto, V.; Sala, M.; Scala, M. C.; Smaldone, G.; Di Matteo, F.; Novi, S.; Tecce, M. F.; Moltedo, O.; Bifulco, G.; Campiglia, P.; Gomez-Monterrey, I. M.; Snoeck, R.; Andrei, G.; Ostacolo, C.; Bertamino, A. Identification of a dual acting SARS-CoV-2 proteases inhibitor through in silico design and step-by-step biological characterization. *Eur. J. Med. Chem.* **2021**, *226*, 113863.
- (90) Weglarz-Tomczak, E.; Tomczak, J. M.; Talma, M.; Burda-Grabowska, M.; Giurg, M.; Brul, S. Identification of ebsele and its analogues as potent covalent inhibitors of papain-like protease from SARS-CoV-2. *Sci. Rep.* **2021**, *11*, 3640.
- (91) Zmudzinski, M.; Rut, W.; Olech, K.; Granda, J.; Giurg, M.; Burda-Grabowska, M.; Zhang, L.; Sun, X.; Lv, Z.; Nayak, D.; Kesik-Brodacka, M.; Olsen, S. K.; Hilgenfeld, R.; Drag, M. Ebsele derivatives are very potent dual inhibitors of SARS-CoV-2 proteases - PLpro and Mpro in in vitro studies. *bioRxiv* **2020**, DOI: 10.1101/2020.08.30.273979v1.
- (92) Cheng, K. W.; Cheng, S. C.; Chen, W. Y.; Lin, M. H.; Chuang, S. J.; Cheng, I. H.; Sun, C. Y.; Chou, C. Y. Thiopurine analogs and mycophenolic acid synergistically inhibit the papain-like protease of Middle East respiratory syndrome coronavirus. *Antiviral Res.* **2015**, *115*, 9–16.
- (93) Chou, C. Y.; Chien, C. H.; Han, Y. S.; Prebanda, M. T.; Hsieh, H. P.; Turk, B.; Chang, G. G.; Chen, X. Thiopurine analogues inhibit papain-like protease of severe acute respiratory syndrome coronavirus. *Biochem. Pharmacol.* **2008**, *75*, 1601–1609.
- (94) Swaim, C. D.; Dwivedi, V.; Perng, Y.-C.; Zhao, X.; Canadeo, L. A.; Harastani, H. H.; Darling, T. L.; Boon, A. C. M.; Lenschow, D. J.; Kulkarni, V.; Huibregtse, J. M. 6-Thioguanine blocks SARS-CoV-2 replication by inhibition of PLpro. *iScience* **2021**, *24*, 103213.
- (95) Brewitz, L.; Kamps, J.; Lukacik, P.; Strain-Damerell, C.; Zhao, Y.; Tumber, A.; Malla, T. R.; Orville, A. M.; Walsh, M. A.; Schofield, C. J. Mass spectrometric assays reveal discrepancies in inhibition profiles for the SARS-CoV-2 papain-like protease. *ChemMedChem* **2022**, No. e202200016.
- (96) Meister, T. L.; Bruggemann, Y.; Todt, D.; Conzelmann, C.; Muller, J. A.; Gross, R.; Munch, J.; Krawczyk, A.; Steinmann, J.; Steinmann, J.; Pfaender, S.; Steinmann, E. Virucidal efficacy of different oral rinses against severe acute respiratory syndrome coronavirus 2. *J. Infect. Dis.* **2020**, *222*, 1289–1292.

- (97) Xu, C.; Wang, A.; Hoskin, E. R.; Cugini, C.; Markowitz, K.; Chang, T. L.; Fine, D. H. Differential effects of antiseptic mouth rinses on SARS-CoV-2 infectivity in vitro. *Pathogens* **2021**, *10*, 272.
- (98) Jin, Z.; Du, X.; Xu, Y.; Deng, Y.; Liu, M.; Zhao, Y.; Zhang, B.; Li, X.; Zhang, L.; Peng, C.; Duan, Y.; Yu, J.; Wang, L.; Yang, K.; Liu, F.; Jiang, R.; Yang, X.; You, T.; Liu, X.; Yang, X.; Bai, F.; Liu, H.; Liu, X.; Guddat, L. W.; Xu, W.; Xiao, G.; Qin, C.; Shi, Z.; Jiang, H.; Rao, Z.; Yang, H. Structure of M(pro) from SARS-CoV-2 and discovery of its inhibitors. *Nature* **2020**, *582*, 289–293.
- (99) Maiti, B. K. Can papain-like protease inhibitors halt SARS-CoV-2 replication? *ACS Pharmacol. Transl. Sci.* **2020**, *3*, 1017–1019.
- (100) Sargsyan, K.; Lin, C. C.; Chen, T.; Grauffel, C.; Chen, Y. P.; Yang, W. Z.; Yuan, H. S.; Lim, C. Multi-targeting of functional cysteines in multiple conserved SARS-CoV-2 domains by clinically safe Zn-ejectors. *Chem. Sci.* **2020**, *11*, 9904–9909.
- (101) Chen, T.; Fei, C. Y.; Chen, Y. P.; Sargsyan, K.; Chang, C. P.; Yuan, H. S.; Lim, C. Synergistic inhibition of SARS-CoV-2 replication using disulfiram/ebesen and remdesivir. *ACS Pharmacol. Transl. Sci.* **2021**, *4*, 898–907.
- (102) Ampornnanai, K.; Meng, X.; Shang, W.; Jin, Z.; Rogers, M.; Zhao, Y.; Rao, Z.; Liu, Z. J.; Yang, H.; Zhang, L.; O'Neill, P. M.; Samar Hasnain, S. Inhibition mechanism of SARS-CoV-2 main protease by ebesen and its derivatives. *Nat. Commun.* **2021**, *12*, 3061.
- (103) Qiao, Z.; Wei, N.; Jin, L.; Zhang, H.; Luo, J.; Zhang, Y.; Wang, K. The Mpro structure-based modifications of ebesen derivatives for improved antiviral activity against SARS-CoV-2 virus. *Bioorg. Chem.* **2021**, *117*, 105455.
- (104) Lee, H.; Lei, H.; Santarsiero, B. D.; Gatuz, J. L.; Cao, S.; Rice, A. J.; Patel, K.; Szypulinski, M. Z.; Ojeda, I.; Ghosh, A. K.; Johnson, M. E. Inhibitor recognition specificity of MERS-CoV papain-like protease may differ from that of SARS-CoV. *ACS Chem. Biol.* **2015**, *10*, 1456–1465.
- (105) Yang, H.; Li, J.; Wu, Z.; Li, W.; Liu, G.; Tang, Y. Evaluation of Different methods for identification of structural alerts using chemical ames mutagenicity data set as a benchmark. *Chem. Res. Toxicol.* **2017**, *30*, 1355–1364.
- (106) Baez-Santos, Y. M.; Barraza, S. J.; Wilson, M. W.; Agius, M. P.; Mielech, A. M.; Davis, N. M.; Baker, S. C.; Larsen, S. D.; Mesecar, A. D. X-ray structural and biological evaluation of a series of potent and highly selective inhibitors of human coronavirus papain-like proteases. *J. Med. Chem.* **2014**, *57*, 2393–2412.
- (107) Johnston, P. A. Redox cycling compounds generate H₂O₂ in HTS buffers containing strong reducing reagents—real hits or promiscuous artifacts? *Curr. Opin. Chem. Biol.* **2011**, *15*, 174–182.
- (108) Soares, K. M.; Blackmon, N.; Shun, T. Y.; Shinde, S. N.; Takyi, H. K.; Wipf, P.; Lazo, J. S.; Johnston, P. A. Profiling the NIH small molecule repository for compounds that generate H₂O₂ by redox cycling in reducing environments. *Assay Drug Dev. Technol.* **2010**, *8*, 152–174.
- (109) Baell, J. B.; Nissink, J. W. M. Seven Year Itch: Pan-assay interference compounds (PAINS) in 2017—utility and limitations. *ACS Chem. Biol.* **2018**, *13*, 36–44.
- (110) Dahlin, J. L.; Walters, M. A. How to triage PAINS—full research. *Assay Drug Dev. Technol.* **2016**, *14*, 168–174.
- (111) Dahlin, J. L.; Nissink, J. W.; Strasser, J. M.; Francis, S.; Higgins, L.; Zhou, H.; Zhang, Z.; Walters, M. A. PAINS in the assay: chemical mechanisms of assay interference and promiscuous enzymatic inhibition observed during a sulfhydryl-scavenging HTS. *J. Med. Chem.* **2015**, *58*, 2091–2113.